Experimental study of the indoor aerosol-dynamics for a low-momentum ventilation system with an air purifier unit

Andreas Westhoff[a], Andreas Kohl[a], Pascal Lange[a,*], Axel Müller[b,]

[a] *German Aerospace Center, Bunsenstr. 10, 37073 Göttingen, Germany*
[b] *OHB System AG, Manfred-Fuchs-Str. 1, 82234 Wessling, Germany*

Abstract

We present an experimental study on the aerosol-dynamics within a test setup representing a class or conference room situation. To ensure realistic flow patterns, the blockage and heat release of the persons are simulated using 18 thermal manikins. The aerosol source is realized by a generator, attached to a thermal manikin, providing a realistic exhalation of artificial saliva. Two different ventilation scenarios are studied regarding aerosol concentration distribution and removal-efficiency. Additionally, the influence of a mask attached to the source and the effect of a moving person on the resulting aerosol concentrations are investigated.
Time and spatially resolved concentrations are measured using 61 particulate matter sensors, installed on three height levels. The ventilation scenarios comprise window opening and a low-momentum ventilation concept, where the air is extracted underneath the ceiling and reenters purified (HEPA14) on floor level. Each of the examined counter measures (open-window, low-momentum ventilation and mask) resulted in a significant lower particle concentration compared to the reference scenario. The low-momentum ventilation with an air purifier unit provided the best aerosol removal-efficiency with a decrease in concentration of up to 96%, followed by the window opening with 60%. The buoyancy flow induced by the heat loads and the resulting flow field caused by the low-momentum ventilation concept lead to well-directed particle transport towards the ceiling. Consequently, a large amount of aerosol was extracted and filtered by the ventilation system resulting in lower particle concentrations. However, local concentrations were strongly depended on the position of the aerosol source.

Keywords: aerosol dynamics, indoor airflow, low-momentum ventilation, air purifier, mask, open-window ventilation

*Corresponding author
Email address: pascal.lange@dlr.de (Pascal Lange)

Nomenclature

$\dot{Q}$	heat flux [W]
$\dot{V}$	volumetric flow rate [cm^3/s]
$\dot{V}_h$	volumetric flow of an exhaling human [cm^3/s]
$\dot{V}_s$	volumetric flow of the source [cm^3/s]
d	particle diameter [µm]
H, h	height [m]
L	length [m]
N	particle number concentration [cm^{-3}]
n	normalised particle number concentration [−]
N_0	scaled particle number concentration of the source [cm^{-3}]
N_s	source particle number concentration [cm^{-3}]
T	time period [s]
t	time [s]
W	width [m]
AC	air change [-]
ACP	air change period [s]
ACR	air change rate [h^{-1}]
LMV	low-momentum ventilation
MB	moving body
OWV	open-window ventilation
TM	thermal manikin
$\Delta N/\mathsf{ACP}$	change rate [cm^{-3}/s]
Γ	decay time [s]
Γ_i/ACP	removal factor [-]
$\sigma(\tau)/\tau$	particle density fluctuation [-]
τ	decay constant [cm^{-3}]
Θ	temperature [°C]
i	sensor position
ex	exhale
max	maximum
min	minimum
ref	reference scenario

1. Introduction

The respiratory disease caused by syndrome coronaviruses (SARS-CoV-2) is the reason for a variety of adverse health effects (Leung et al., 2020) with a mortality rate currently estimated at 1.4% - 3.2% (Bialek et al., 2020). The transmission of the virus is due to airborne transmission or smear infection. In general, the two primary airborne transmissions of respiratory pathogens are droplet transmission over short-range (between 2 or 3 meters) and long-range transmission via aerosols Tellier (2009). Regarding smear infection the transmission is often through contact e.g. touching a contaminated surface followed by contact with mucous membranes of the eyes, nose or mouth, due to droplet inhalation in nasal/upper airway, or aerosol transmission due to inhalation into upper or lower airways (Tellier et al., 2019). For influenza transmission, it has been controversial which mode of transmission is predominant (Tellier, 2009; Brankston et al., 2007). However, in case of SARS-CoV-1 and SARS-CoV-2, the fact that aerosols are a dominating mode of transmission is now largely uncontroversial, as Kohanski et al. (Kohanski et al., 2020) point out in their article. Since both SARS-CoV-1 and SARS-CoV-2 in humans target the surface receptor angiotensin-converting enzyme-2 (ACE-2) as a port of entry and ACE-2 is expressed on type II pneumocytes in the lung as well as on cells of the nasal mucosa, a transmission route via aerosols appears to be a plausible

mechanism. Moreover, there is an overwhelming evidence that indoor airborne-transmission is strongly associated with virus loaded aerosol droplets. Hence, indoor aerosol-dynamics play a dominant role in the spread of the corona virus disease (COVID-19) (Morawska & Milton, 2020; Jayaweera et al., 2020; Buonanno et al., 2020; Zhang et al., 2020; Hwang et al., 2021; de Man et al., 2021; Furuse et al., 2020). Especially in case of super-spreading events (Kolinski & Schneider, 2021; Lakdawala & Menachery, 2021; Miller et al., 2021; Hamner, 2020), which always seem to occur indoors (Nishiura et al., 2020).

Because the virus is too small to be transported from one person to another directly, droplets exhaled by the human carry the virus load. Hence, the characterisation and specification of indoor aerosol-transport, taking into account indoor flow conditions, including thermal and forced convective airflow, are key elements for infection risk understanding and prevention in the case of COVID-19 transmission (Mittal et al., 2020; Rangel, 2021; Moritz et al., 2021; Al Huraimel et al., 2020). Hence, many public health decisions (e.g. protective equipment, control strategies, communication with the public) depend on quantitative estimates of aerosol research activities conducted in collaboration with the medical community. The emission rates of respiratory droplets, their size distribution, their mechanisms of formation inside and outside the infected host, their dispersion and transport in still air and ventilated indoor environments are topics in this regard, which are particularly well placed to provide data to contribute to informed public health decisions and the well-being of our society. As a result, a plethora of guidelines have been published in order to minimise the risk of infections due to the transmission of COVID-19 in rooms and buildings (Bazant & Bush, 2021, 2020; Morawska et al., 2020; Peng et al., 2021; Tang et al., 2021). An early study was published by Azimi et al., who demonstrate the importance of aerosol transmission in the case of the Diamond Princess cruise ship (Azimi et al., 2021). They note that more than 50 per cent of SARS-CoV-2 transmission on the ship occurred through aerosol inhalation, both at close contact and at long distance. This emphasize the need for measures aimed at controlling aerosol inhalation, in addition to those already installed to control larger droplets by wearing a mask or keeping distance. Other studies such as Azuma et al. (Azuma et al., 2020) as well as (Morawska et al., 2020) examined the environmental factors which are important for SARS-CoV-2 transmission. They present engineering controls to prevent or minimize SARS-CoV-2 transmission in indoor environments and note that indoor ventilation should be recognised as an established method to reduce airborne transmission.

With the objective to verify in which way the ventilation influences the aerosol dynamics and which control strategies are suitable for reducing the aerosol concentration, different concepts have been investigated. In this paper, we consider the issue of indoor aerodynamics from the point of view of whether a low-momentum ventilation (LMV) system with an air purifier, an open-window ventilation (OWV) or a medical (FFP2) mask can reduce aerosol concentrations or prevent an uncontrolled propagation of aerosols in a room resulting in a reduced risk of infection. For this purpose, we studied the aerosol dynamics emphasising the range from 0.3 µm up to 2.5 µm aerodynamic diame-

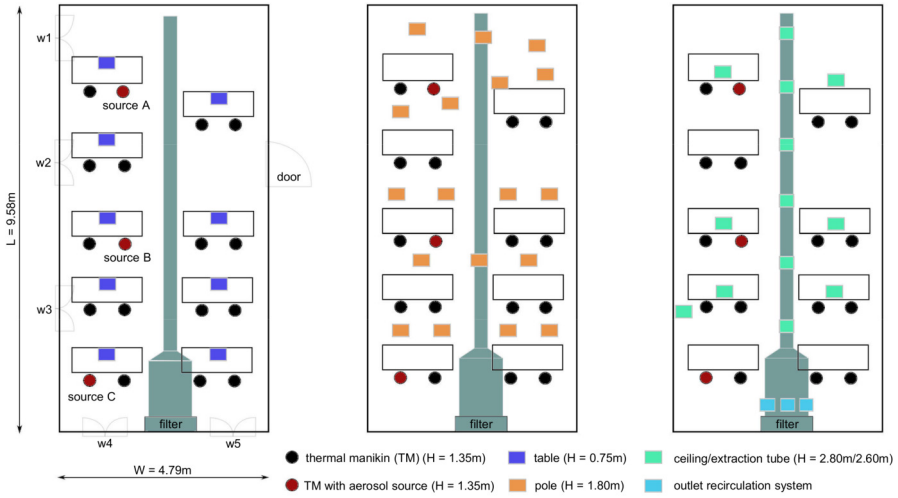

Figure 1: Floor plan of the test environment (class room) with the recirculation system and the corresponding positions of the particle sensors. The windows to the outside are labled W1 - W5. The unfilled squares indicate the tables, the filled circles the TMs, which are equipped with a particle sensor. The height positions H of the particle sensors are indicated in brackets.

ter. This range covers the particle sizes of interest emitted by a human during respiration (Nazaroff, 2016; Johnson et al., 2011; Jones & Brosseau, 2015).

The present paper is structured as follows: the section experimental set-up introduces the test environment and the measurement methods comprising the used thermal manikins, the aerosol generator and the used sensor for measuring local aerosol densities. It is followed by the presentation and analysis of the latest results. Finally, the paper ends with a conclusion and discussion on the effectiveness of control strategies and its consequences for indoor ventilation.

2. Experimental Setup

2.1. Test-Environment

Measurements of the aerosol dynamics are performed in a room representing a class- or conference room equipped with a recirculation air system, which includes a HEPA14-filter. Figure 1 illustrates the floor plan of the test room with the corresponding positions of the particulate sensors, the table arrangement and the positions of the thermal manikins (TM). The dimensions of the room are $L = 9.58\,\mathrm{m}$ in length, $W = 4.79\,\mathrm{m}$ in width and $H = 2.89\,\mathrm{m}$ in height. This gives a base area of $A = 46\,\mathrm{m}^2$ and a volume of $V = 130\,\mathrm{m}^3$. On the left side of the room are three windows (w1, w2, w3), two on the back (w4, w5) and a door on the right side. The recirculation system (Up-Wind 900 by the HT-group), wich serves as LMV system, is coloured grey. It consists primarily of: a ceiling-mounted extraction tube that extends approximately the length of the room,

speed-controlled fans for the supply of recirculated air with a defined volume flow rate of up to $\dot{V} = 950\,\mathrm{m}^3/\mathrm{h}$ and a floor-level air outlet with a HEPA14-filter. Figure 2 shows a photograph that gives an overview of the setup with the recirculation system. By means of the ventilation system, we are able to provide a reproducible and controlled ventilation. Here the filtered air leaves the recirculation system through the outlet near the floor with a low momentum and rises due to the buoyancy flow induced by the TMs. Finally, the ascended air is discharged through the extraction tube at the ceiling. In addition, the system is equipped with a silencer to reduce noise emission to 40 dB and lower.

The room is equipped with tables and seats. The positions of the tables, each with two seats, are illustrated in figure 1 as unfilled squares and the circles indicate the position of the seats with the TMs. Furthermore, the red filled circles (●) represents the aerosol exhaling TMs. All TMs are seated on chairs near the tables (see figure 2). For the present investigation, the function of the TMs are twofold: first, they are an obstacle that represents a seated person, equipped with a particle sensor in the region of the nose/mouth to analyse the potentially inhaled aerosol by that person and second, they simulate the sensible heat release of a human body (see figure 3d). The TM's core is made of melamine resin foam, which is wrapped with a resistance wire and is additionally covered by a thin layer of black thermally conductive aluminium. Moreover, in order to generate a realistic heat emission for a lightly clothed person with different heat-flux densities for the body parts, the winding distances of the heating wire are individually designed (Lange et al., 2018). For the present investigation each TM has a sensible heat release of $\dot{Q}_{\mathrm{TM}} = 75\mathrm{W}$ to ensure heat loads comparable to a sitting person in rest. In general and especially here, the experimental simulation of realistic heat loads is of utmost importance for the generation of realistic buoyancy flows in the room.

With the objective to verify the dynamics of the aerosol concentration, particulate sensors are distributed equally in the room on three height levels. Further sensors are attached on the face of the TMs (see figure 2). In case of the TM's face, the sensors are located at a height of $h_{\mathsf{s}}^{\mathsf{TM}} = 1.35\mathrm{m}$. The positions of the sensors in the test room are depicted in figure 1, where the coloured squares represent the sensors on the three different height levels: (■) on the table $h_{\mathsf{s}}^{\mathsf{table}} = 0.75\mathrm{m}$, (■) on poles at a height of $h_{\mathsf{s}}^{\mathsf{pole}} = 1.80\mathrm{m}$ and (■) at the ceiling as well as on the underside of the extraction tube at a height of $h_{\mathsf{s}}^{\mathsf{ceiling}} = 2.80\mathrm{m}$ and $h_{\mathsf{s}}^{\mathsf{tube}} = 2.25\mathrm{m}$, respectively. In addition, sensors (■) are placed at the air outlet right behind the filter (see figure 2 outlet) in order to check that the filter is working as expected and to detect any backflow that could cause the filtered air to mix with the ambient air at the outlet. For this purpose, there is one sensor in the centre of the diffuser and two sensors are on the left and right side of the outlet, respectively.

2.2. Aerosol generation and detection

For the experimental simulation of a realistic aerosol exhalation, an aerosol generator was developed at the DLR in Göttingen. Figure 3a shows the generator, which basically consists of a dispersion and a settling/mixing cham-

Figure 2: Photography of the test setup showing the installed particulate sensors, the TMs and the ventilation system with the extraction tube at the ceiling and the air outlet at the floor level.

ber. The dispersion chamber is a sealed housing containing an airbrush gun (AFC-101A) with a nozzle of 0.35 mm in diameter and a reservoir for artificial saliva. The artificial saliva (mixed according to NRF 7.5 (Arzneimittel-Codex, 2007)) is composed of: potassium chloride (0.12g), sodium chloride (0.085g), sodium monohydrogen phosphate dodecahydrate (0.25g), calium chloride dihydrate (0.015g), magnesium chloride hexahydrate (0.005g), sorbic acid (0.1g), carmellose sodium 400 (0.5g), sorbitol solution (4.3g) and aqua purified add (100.0g). Further, the aerosol generator is connected to a facial mask (see fig. 3b and 3c) to generate a realistic mouth-nose exhalation. To produce a defined, constant and homogeneous mass-flow of the dispersed saliva the system is equipped with a particulate matter sensor and a compressed air regulator to control and monitor the aerosol flow. By means of this configuration a precisely defined aerosol exhalation can be simulated.

The spatial and temporal distribution of the aerosol concentration is measured with SPS30 particulate matter sensors by Sensirion. These laser-based sensors detect and count particles by means of light scattering. In particular, a continuous stream of air is passing the device, which transports ambient air into the measurement volume. From a signal of a photo diode measuring the light intensity, the particle number concentrations are calculated for the internal volume. The concentration are binned for particle diameter ranges of 0.3 µm - 0.5 µm, 0.5 µm - 1.0 µm, 0.3 µm - 2.5 µm, 0.3 µm - 4.0 µm and 0.3 µm - 10.0 µm. Further, it should be noted that just for the range 0.3 µm - 2.5 µm

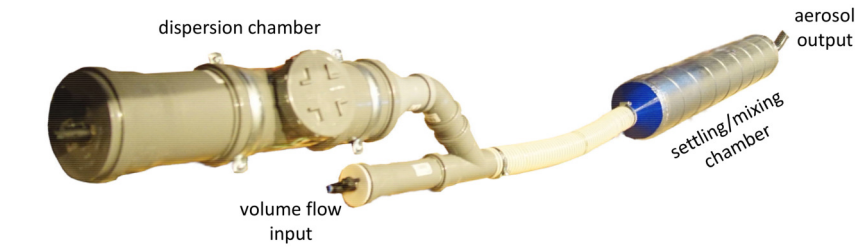

(a)

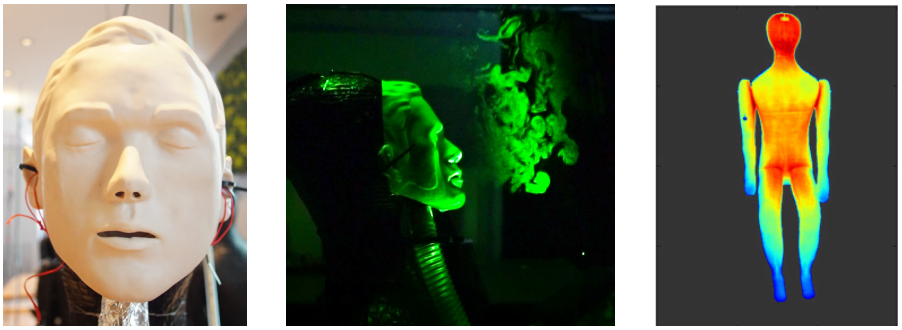

(b) (c) (d)

Figure 3: (a)Aerosol generator, (b) TM with a mask for aerosol exhalation through the nose/mouth, (c) laser-visualisation of the exhaled saliva dispersion, (d) infrared thermography of the heated TM.

the concentration is directly retrieved from the light signal. The concentrations for the particle diameter $d > 2.5\,\mu m$ is estimated using the distribution profile of all measured particles. Since the refractive index of the suspended particle is unknown to the sensor, the measured particle sizes depend on the particle materials. However, saliva with the same composition is always used in these measurements, so this has no influence on the comparability and meaningfulness of the results. Moreover, a self-cleaning mode ensures a consistent and validated data acquisition, especially for long-term measurements. Regarding the accuracy of the SPS30 sensors, Tryner et al. (Tryner et al., 2020) compare the results of the SPS30 as well as other low-cost particulate matter sensors with a direct mass transducer. They found that the sensor is insensitive to changes in relative humidity, operates stably over long measurement periods and performs best, compared to the other sensors tested.

An in-house data-acquisition system is used to record sensor data and monitor the experiment. The system uses the serial protocols such as UART, SPI or I2C to a central host device that stores the measurement data. It is designed to acquire data from more than 100 sensors with frequencies up to 20Hz. In addition, robustness is ensured by using easily replaceable and well-tested standard components.

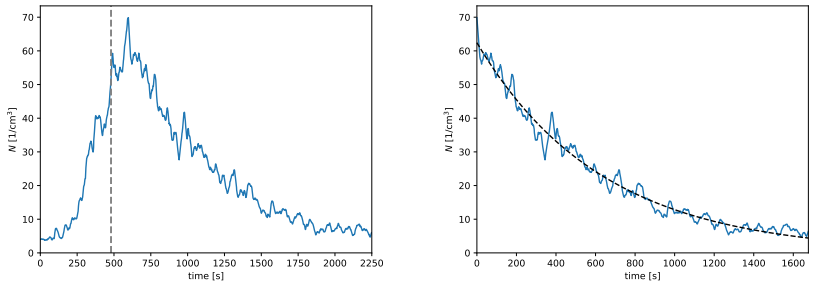

(a) (b)

Figure 4: Aerosol concentration for the sensor located in the face of the TM: (a) time series for the particle number concentration for the entire measurement period and (b) exponential decrease of the concentration for the decay period.

3. Measurement procedure

With the objective to investigate the dispersion of aerosol, emitted from a source, a dedicated measurement procedure and evaluation method is defined in order to verify the aerosol dynamics in the room for different scenarios. All measurements are performed for a mean room-temperature of $\Theta_r = 24(1)\,^{\circ}\mathrm{C}$ except the open-window scenario, where the air temperature is strongly affected by the outdoor air temperature. The corresponding measurement procedure is described with the help of the following diagrams.

For all scenarios, the measuring time of $T = 2400\,\mathrm{s}$ is divided in an exhaling and a decay period. Figure 4a shows a typical time series of a single sensor (located at the face of the TM) measuring the particle number concentration N for the diameter range of $0.3\,\mu\mathrm{m} \leq d \leq 2.5\,\mu\mathrm{m}$ as a function of time for a scenario with air-filtering by LMV. The dashed grey vertical line indicates the boundary between the exhalation- and the decay period. The investigations start with the exhale period $T_{\mathsf{ex}} = 480\,\mathrm{s}$, where at the beginning the particle background-concentration has its minimum. This period will be referred to as interval A in the following. During this period, the source exhales aerosol continuously, consisting of air and dispersed artificial saliva. The volumetric flow rate of the source amounts to $\dot{V}_s = 200.0\,\mathrm{cm^3 s^{-1}}$, which is only the half of the typical human expiratory peak flow $\dot{V} = 400\,\mathrm{cm^3 s^{-1}}$ (Gupta et al., 2010). The reason for halving the volume flow is, that it is not intended to simulate a complete sinusoidal breathing cycle. Rather, the aim is to simulate the momentum of the exhaled air as realistically as possible. To this end, the TM exhales continuously at around double of a typical human volume flow $\dot{V}_h \approx 100.0\,\mathrm{cm^3 s^{-1}}$ through the mouth and nose. In addition, the air jets from the nose are tilted downwards from the horizontal by about 45^o and maintain a distance angle of 30^o from each other (Melikov & Kaczmarczyk, 2007; Kohl et al., 2021). By means of

this configuration we are able to simulate the effect that the human exhaled air jets tend to descend first and rise afterwards due to buoyancy caused by the temperature difference between the exhaled air and the ambient temperature, that is usually lower (Bjørn & Nielsen, 2002).

In real breathing, the exhaled air jets from the mouth and nose are much more complex. For the present investigation, however, the exact aerosol dynamics in the vicinity of the face is less of interest for the global aerosol dynamics. The focus is rather on the aerosol propagation within the test environment. Therefore, this simplified experimental simulation of exhaled saliva particles is sufficient for this purpose. Moreover, the averaged concentration of exhaled aerosol in the face area of the source (roughly $N > 2000\,\mathrm{cm}^{-3}$) is several orders of magnitude larger compared to the density in human respiration ($N \approx 1\,\mathrm{cm}^{-3}$) (Morawska et al., 2009; Gaeckle et al., 2020; Johnson et al., 2011). For the measurements this high number concentration of droplets is needed for a sufficient measuring signal of the particle sensors at each sensor position.

At the end of this period, the exhaling is stopped and the decay period begins with a length of $T_{\mathsf{ex}} = 1770\,\mathrm{s}$ (figure 4b). For this interval, the decrease in particle concentration as a function of time is studied with the objective to verify the spatial transport and the dynamics of the aerosol for the different scenarios. Further, two additional time intervals are defined for this period. The two intervals $480\,\mathrm{s} < t \leq 1080\,\mathrm{s}$ and $2070\,\mathrm{s} < t \leq 2250\,\mathrm{s}$ are referenced as interval B and interval C, respectively. The interval B of 600 s corresponds to an air change (AC) of one, speaking the time which is needed for changing the air volume in the room once, for the case of LMV. The interval C represents the average residual number concentration at the end of the entire measurement time. Furthermore, in case of LMV with air purifier an exponential decrease of the aerosol concentration for almost all sensors is found (figure 4b). Based on a characterisation of this exponential decrease an analysis of the aerosol dynamics is performed. A detailed characterisation of the analysis method is given at the beginning of the result section 4.

4. Results

The present study investigates the aerosol dispersion in a room for the following scenarios: LMV-system with air purifier, mask (mouth/nose covering) and open-window ventilation (OWV). With the aim to characterise the impact of these measures on the aerosol dynamics and the corresponding saliva spreading in the test room, the time series of the particle number concentration determined by the particulate sensors is analysed as described below.

For reason of comparability, the measured aerosol concentration is normalised according to equation 1 using the source particle flow.

$$N_0 = \frac{N_\mathrm{s}\,\dot{V}_\mathrm{s}}{\dot{V}_\mathrm{h}} \tag{1}$$

Here, N_s denotes the number density determined in the settling chamber of the

particle generator, $\dot{V}_\mathrm{s}$ the volumetric flow of the source and $\dot{V}_\mathrm{h}$ the characteristic volumetric flow of an exhaling human (details see sec. 3). To verify the impact of the aerosol dispersion for the different studied scenarios with respect to the particle number density for the so-called reference cases N_ref, the density N is given as $1 - n/n_\mathsf{ref}$. This value represents the change in relation to the corresponding reference case, where $n = N/N_0$ and $n_\mathsf{ref} = N_\mathsf{ref}/N_0^\mathsf{ref}$. In the following, the term reference case refers to the respective scenario without any control strategies to reduce the aerosol concentration and to prevent the spread of droplets in the room.

To verify the effectiveness of the LMV-system regarding the transport of aerosol in direction to the ceiling as well as the removal rate, the time series starting at the beginning of interval B is analysed. Therefore, a curve fitting with an exponential function (see figure 4b) is performed.

$$N(t) = \tilde{N}\, e^{-\tau\, t} + \mathcal{C}, \tag{2}$$

the fitting parameters $\tilde{N}$, τ, and $\mathcal{C}$ of the underlying equation (see 2) are calculated by means of a least-square algorithm. Based on these parameters, decay time Γ is calculated for each sensor position,

$$\Gamma_i = -\frac{1}{\tau_i} \ln\left(\frac{0.2\overline{N}_\mathsf{max}}{\tilde{N}_i}\right), \tag{3}$$

where $\overline{N}_\mathsf{max}$ denotes the maximum aerosol concentration (average over all sensor position) at the beginning of interval B and i denotes the sensor position. In addition, the uncertainties of the fitting parameters are determined by means of the covariance matrix M_{cov}

$$\sigma(\tilde{N}), \sigma(\tau), \sigma(\mathcal{C}) = \sqrt{\mathsf{diag}(M_\mathsf{cov})}. \tag{4}$$

Further, with the help of Γ and $\sigma(\tau)$, the following criteria are defined to characterise the aerosol dynamics: the removal factor Γ_i/ACP, the fluctuations $\sigma(\tau)/\tau$ and the aerosol flow $\Delta N/\mathsf{ACP}$, where

$$\Delta N = \int_{t(N_\mathsf{max})}^{\mathsf{ACP}} \dot{N} \mathsf{d}t. \tag{5}$$

The removal factor Γ_i/ACP as well as the aerosol flow $\Delta N/\mathsf{ACP}$ represents the measures: how many ACs are necessary to achieve a particle concentration of $0.2\overline{N}_\mathsf{max}$ starting from the time N_max and the mean concentration change for the time span of one air change period (ACP) of one AC, respectively. In addition, the fluctuation $\sigma(\tau)/\tau$ describes how much the time series differs from a theoretical undisturbed transport, represented by the exponential function 2. It serves as an evaluation criterion to characterise the stability of the aerosol transport in the direction of the tube at the ceiling or towards the open windows. Here, large values indicate increased dynamics while lower values are characteristic

for a reduced air movement, respectively.

The following result section is divided into three parts. In the first part 4.1, the results of the spatial distribution of the particle concentration are presented while the second part 4.2 discusses the results for the aerosol dynamics in case of the LMV. In part 4.3, the results of all measurements are discussed and compared addressing the aerosol concentration and aerosol removal rate.

4.1. Spatial aerosol distribution

4.1.1. Reference

In the following the results of aerosol dispersion for the reference cases without any control strategy are discussed. The function of these measurements is twofold. Firstly, the results are used to analyse the spatial distribution of the aerosol concentration and secondly, to compare the different flow scenarios with the reference cases, serving as a normalisation factor.

Figure 5 and 6 reveal the spatial distribution of the time-averaged number concentration N/N_0 in percent with respect to the reference cases for interval A and B, respectively. Here and in the following, the different sensor heights are shown from left to right: the lower level represents the sensors located on the forehead of the TMs and on the top of the table, the middle level the sensors at a height of $h_{\mathsf{s}}^{\mathsf{pole}} = 1.80\,\mathrm{m}$ and the ceiling level the sensors at the ceiling and at the underside of the extraction tube at a height of $h_{\mathsf{s}}^{\mathsf{ceiling}} = 2.80\,\mathrm{m}$ and $h_{\mathsf{s}}^{\mathsf{tube}} = 2.25\,\mathrm{m}$, respectively. In addition, the positions of the corresponding sources are highlighted in blue and the normalised particle concentration is colour-coded. The time-averaged aerosol concentration for interval A is shown in figure 5 as a function of source position. For all source positions, a significant increase in particle concentration is found. Up to $0.17\% \times N_0$ in the vicinity of the exhaling TM. In particular, at the middle level near the source, the buoyancy flow induced by the TM causes a rise of the exhaled aerosol in the direction of the ceiling. Furthermore, for the two cases where the source is placed on the aisle chair, the TMs sitting at the same table (sensor S02 for source A and sensor S08 for source B) are significantly less affected by about $0.07\% \times N_0$ than source C where the TM sits at the window side. Here, the concentration at sensor position S15, located at the TM's forehead on the right side, is $0.15\% \times N_0$. This is twice as high in comparison to the cases where the source is located on an aisle seat.

This result illustrates that the particle-concentration distribution and thus the propagation depends strongly on the source position and the current flow conditions. For the entire room, it seems that a large-scale flow structure from the front to the back is present, leading to elevated values behind the source A and source B in case of interval A. However, this flow is not representative for every comparable configuration and depends on the individual boundary conditions. Nevertheless, two general effects are obvious. The vertical buoyancy flow induced by the TMs leads to a rising of the exhaled aerosol and the large-scale flow leads to an additional spreading. The spatial distribution for interval B as a function of the source position is illustrated in figure 6. It depicts the

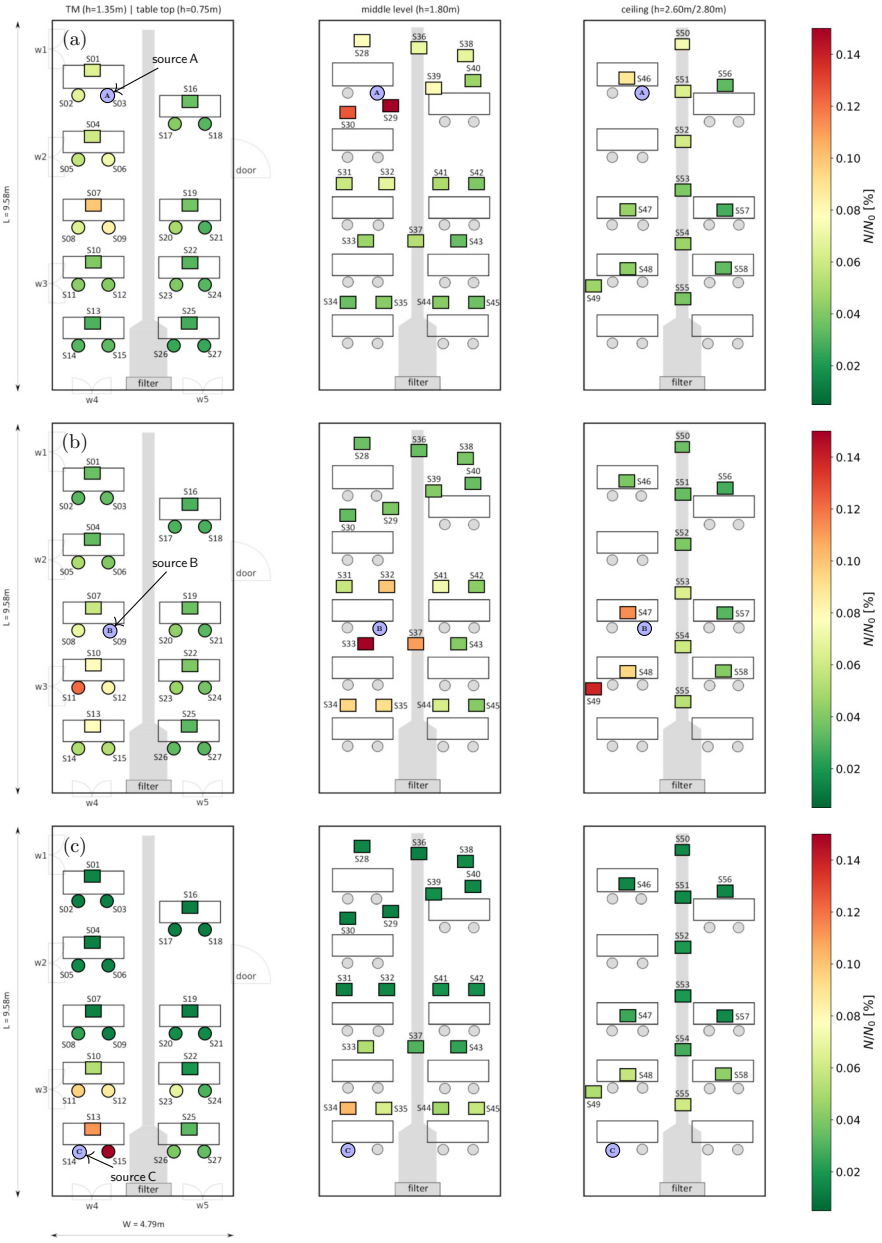

Figure 5: Time-averaged and normalised particle number concentration N/N_0 in percent for interval A for three different source positions: (a) source A, (b) source B and (c) source C.

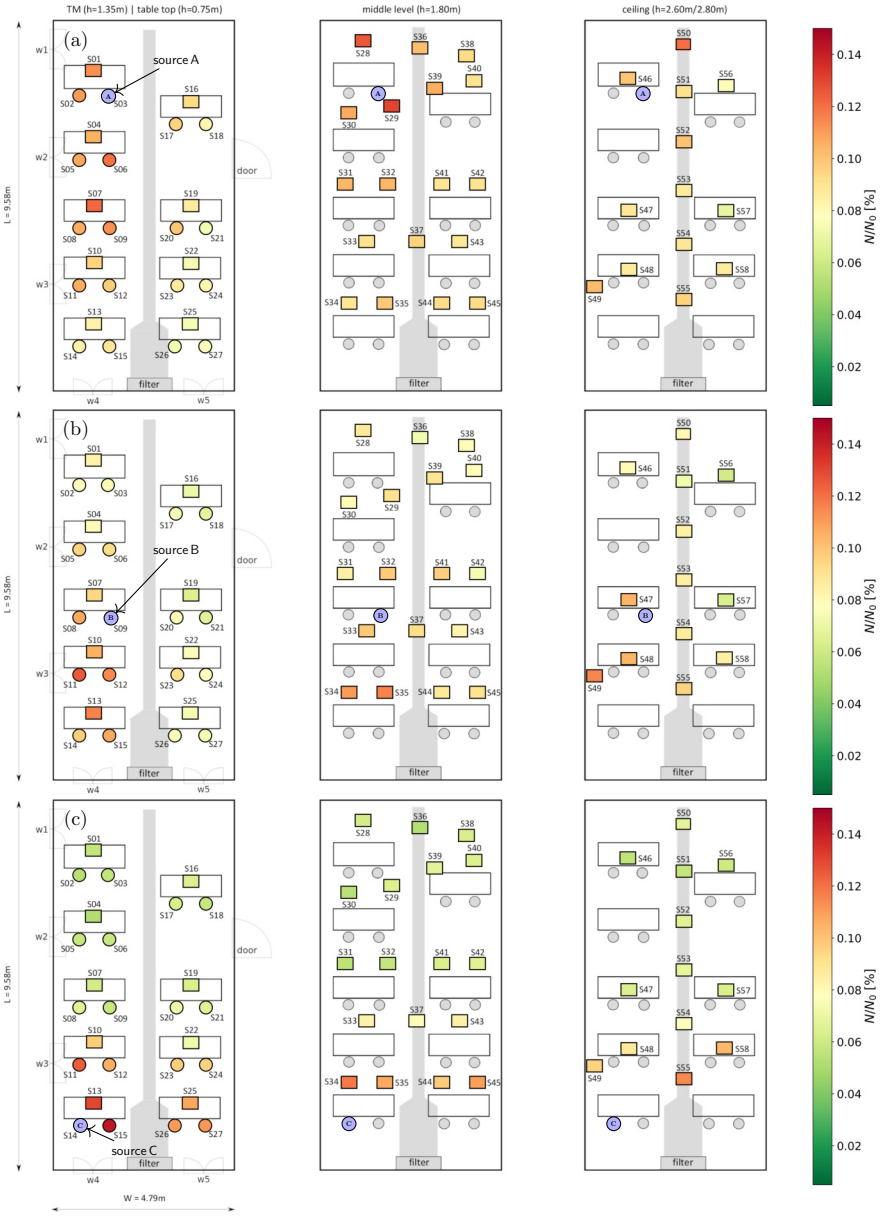

Figure 6: Time-averaged and normalised particle number concentration N/N_0 in percent for interval B for three different source positions: (a) source A, (b) source B and (c) source C.

Figure 7: Time-averaged and normalised particle number concentration N/N_0 in percent over interval C for source location A.

time-averaged distribution of the particles for the time period after stopping the exhalation and reveals how the aerosol propagates in the room without any ventilation. It can be seen that the particles spread in the whole room within a period of 10 min and the propagation depends on the source position. Furthermore, for source A and source B an aerosol transport is observed from front to back, which leads to higher concentration on the left side for the lower height level behind the source A and source B. However, in case of source C, higher values are located in the back-left corner. In addition, the buoyancy flow induced by the TMs at the positions source A and source C leads to increased values in the middle plane and in the ceiling area in the front and back area, respectively. For source B, which is located almost in the centre of the room, increased concentrations are found at the higher measurement positions near of the source as well as at the seat positions right behind the source B.

At the end of the measurement time, the particles are almost homogeneously distributed in the room due to thermal convective airflow induced by the TMs. Figure 7 shows the particle number concentration N/N_0 time-averaged over the interval C for the case of source A, revealing the number concentration is almost similar for all sensor positions. Comparable results are also found for the other two source positions, but not shown here. The concentration, spatially averaged over all sensor positions, amounts to $\overline{N}_{\mathsf{A}} = 0.072(5)\,\% \times N_0$ for source A, $\overline{N}_{\mathsf{B}} = 0.073(4)\,\% \times N_0$ for source B and $\overline{N}_{\mathsf{C}} = 0.071(4)\,\% \times N_0$ for source C. Consequently, for the reference cases a homogeneous particle distribution with about 0.07% of the particles exhaled by the source is obtained.

In conclusion, the aerosol distribution in a room is determined by the superposition of the large-scale flow structures in the room and the thermal convective flow induced by the heat loads i.e. human body. This results in a plethora of flow situations as well as an uncontrolled and partly erratic transport of the aerosol. While at the beginning of the investigation period (< 15 min) the exhaled particles are close to the source, in the following convective airflows lead

to a mixing of the exhaled aerosols with the room air and at the end the particles are homogeneously distributed in the entire room.

4.1.2. Open-window ventilation and mouth/nose mask

(a) (b)

Figure 8: Laser-light visualisation of the aerosol exhaled by a TM with a FFP2 mask.

With the objective to identify the impact of the aerosol distribution in case of currently recommended control strategies (Templeton et al., 2020; Duan et al., 2020) an open-window ventilation (OWV) and the effects of a EN149 FFP2 (FFP = Filtering FacePiece) mask (comparable to KN95 standard) are investigated. The discussion starts with the results for oral and nasal covering. With the objective for evaluating the effectiveness of surgical, FFP2/KN5 or FFP3/KN99 masks in case of SARS-CoV-2, a large number of studies have been conducted. Almost all of these studies have demonstrated a reduction in the likelihood of infection (Atchison et al., 2021; D'Alessandro et al., 2020; Howard et al., 2021). The studies recommend the wear of masks in order to reduce the virus transmission and show an additional self-protection effect for FFP2/KN5 and FFP3/KN99. However, it is difficult to make a general and concrete statement about the extent to which the risk of infection is reduced, as transmission is highly dependent on the boundary conditions and, not at least, the fitting of a mask is of decisive importance (Regli et al., 2021).

The findings of (Regli et al., 2021) regarding the impact of mask fit are consistent with our observations. The pictures in figure 8 show a laser-light visualisation of saliva particles exhaled by a TM wearing a FFP2 mask. The visualisation clearly reveals particles escaping through the gap between mask and nose. It further shows that possible leaks, especially at the nose, strongly influence how much aerosol is released into the environment even though an FFP2 mask is worn. In addition, a smaller amount escape directly through the

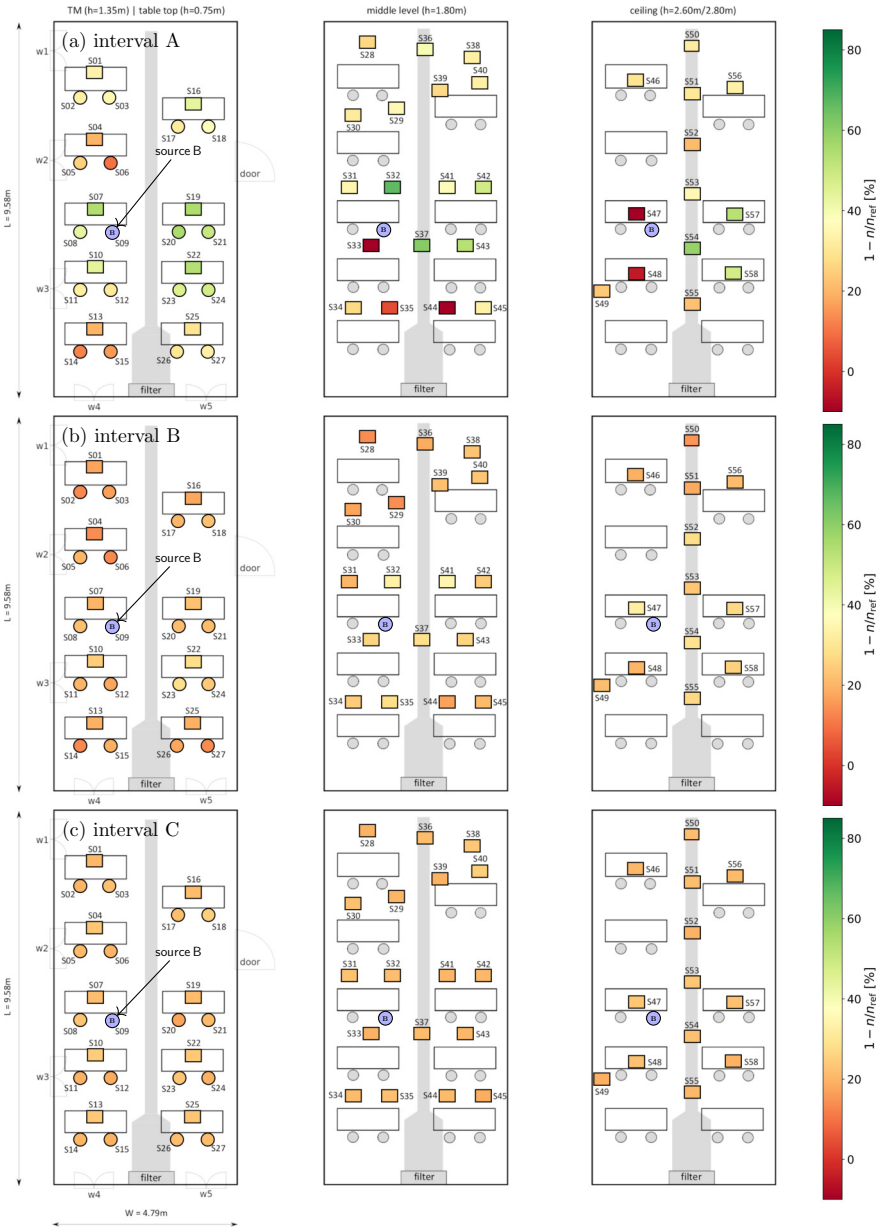

Figure 9: Time-averaged and normalised particle number concentration $1 - n/n_{\mathsf{ref}}$ in percent in case of the source wearing a FFP2 mask for: (a) interval A , (b) interval B and (c) interval C.

mask (see figure 8b on lower right side). However, due to the lower breathing momentum, compared to the case without a mask, the particle flow is primarily buoyancy driven. As a result, an almost vertical flow is observed towards the ceiling. This buoyancy flow directly influences the aerosol distribution, which is shown below.

Figure 9 plots the time-averaged concentration change $1 - n_{\mathsf{mask}}/n_{\mathsf{ref}}$ in percent as a function of the measurement interval. The vertical aerosol motion described earlier is reflected in the spatial distribution (fig. 9a). The image shows $1 - n/n_{\mathsf{ref}}$ during the exhalation period (interval A). On the average, the concentration is 26% lower in comparison to the reference case. In particular on the lower and middle level near the source, particle concentrations up to 67% lower are found. However, significant higher values in relation to the reference case are measured for the sensor positions S33, S44, S47 and S48 with up to 37% higher values for the sensor (S33) located at the middle level behind the source. The reason for the higher values at these positions is that due to the lower momentum of the exhaled air jet getting blocked by the mask, the aerosol motion near the source is buoyancy driven. As a consequence, the aerosol that escapes from the edges of the mask rises directly towards the ceiling in the vicinity of the source and results in higher concentrations at S33, S47 and S48, while the increased values for S44 appear to be the result of large-scale flow structures in the room.

For the interval B an almost homogeneous distribution is observed with a standard deviation of $\sigma^{(B)}(N_{\mathsf{mask}}) = 0.162 \times \overline{N}$. This distribution is comparable to the corresponding reference case with $\sigma^{(B)}(N_{\mathsf{ref}}) = 0.168 \times \overline{N}$. Considering the influence of the mask on the particle concentration with respect to the reference case, figure 9b reveals for all sensor positions lower values of $8.1\% < 1 - n/n_{\mathsf{ref}} < 34.4\%$. In the spatial mean, the concentration is reduced by 21%. Finally, an almost completely homogeneous distribution is observed for interval C (see Figure 9c) with a standard deviation of $\sigma^{(C)}(N_{\mathsf{mask}}) = 0.06 \times \overline{N}$. In contrast to the reference case, the spatially-averaged concentration is 21% lower, which is similar to interval B and the range is $17.4\% < 1 - n/n_{\mathsf{ref}} < 25.1\%$.

In addition to the influence of a FFP2 mask on the particle concentration, a scenario of an OWV is investigated. Therefore, the exhaling period (interval A) is carried out with closed windows. After this period the windows w1 and w3 are opened. The result for the open-window scenario is depicted in figure 10. For interval B a lower particle concentration of $18.2\% < 1 - n/n_{\mathsf{ref}} < 68.2\%$ is obtained at all sensor positions with a spatial average of 52%. The highest load is found in the rear area of the room and especially near window w3. For the front area, the influence by the OWV on the particle concentration is significantly lower compared to the reference case. Here, in particular the sensors S46 and S56 at ceiling level reveal a significant smaller change of just $n/n_{\mathsf{ref}} \approx 20.0\%$. In case of interval C, the concentration is significant lower for all sensor positions with $54.2\% < 1 - n/n_{\mathsf{ref}} < 77.7\%$ and the spatial standard deviation is $\sigma^{(C)}(N_{\mathsf{OWV}}) = 0.137 \times \overline{N}$.

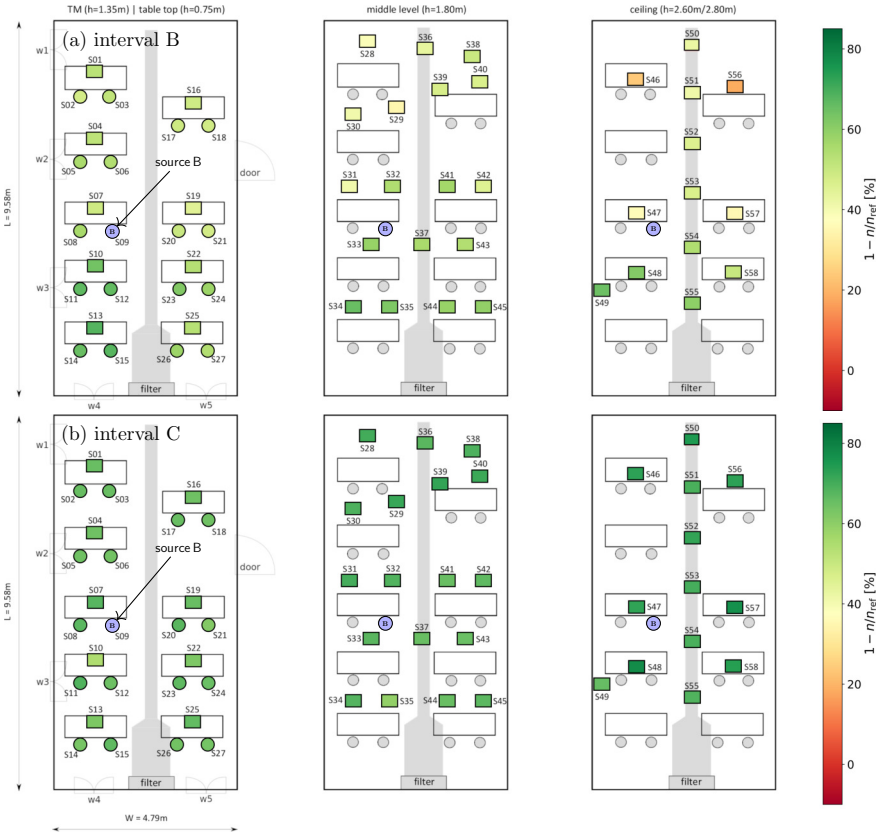

Figure 10: Time-averaged and normalised concentration change $1 - n/n_{\mathsf{ref}}$ in percent in case of the open-window ventilation for: (a) interval B and (b) interval C.

4.1.3. Low-momentum ventilation

In this section, the results of the tests addressing the low-momentum ventilation concept are presented. The system installed serves as a sample configuration to investigate the basic mechanisms of low-momentum ventilation with recirculation and filter system. All measurements are carried out at a volume flow rate of $\dot{V} = 800\mathrm{m}^3/\mathrm{h}$ and the air volume of the test room is approximately $V_{\mathrm{air}} \approx 130\mathrm{m}^3$. Hence, the air change rate amounts to $ACR \approx 6.0\mathrm{h}^{-1}$, which is comparable to other studies on the issue of indoor ventilation in context of COVID-19 like the work of Curtius et al. (Curtius et al., 2021) testing a mobile purifier with a rate of $ACR = 5.7\mathrm{h}^{-1}$. In addition, other measurements have been made at much lower air change rates of $ACR < 3.0\mathrm{h}^{-1}$, such as Blocken et al. (Blocken et al., 2021), who investigate ventilation and air purification in a gym.

Figure 11 shows the time-averaged $1-n/n_{\mathsf{ref}}$ in percent for interval A in case of LMV with air cleaning. Due to the air cleaning, significantly lower aerosol concentrations are found on average compared to the corresponding reference

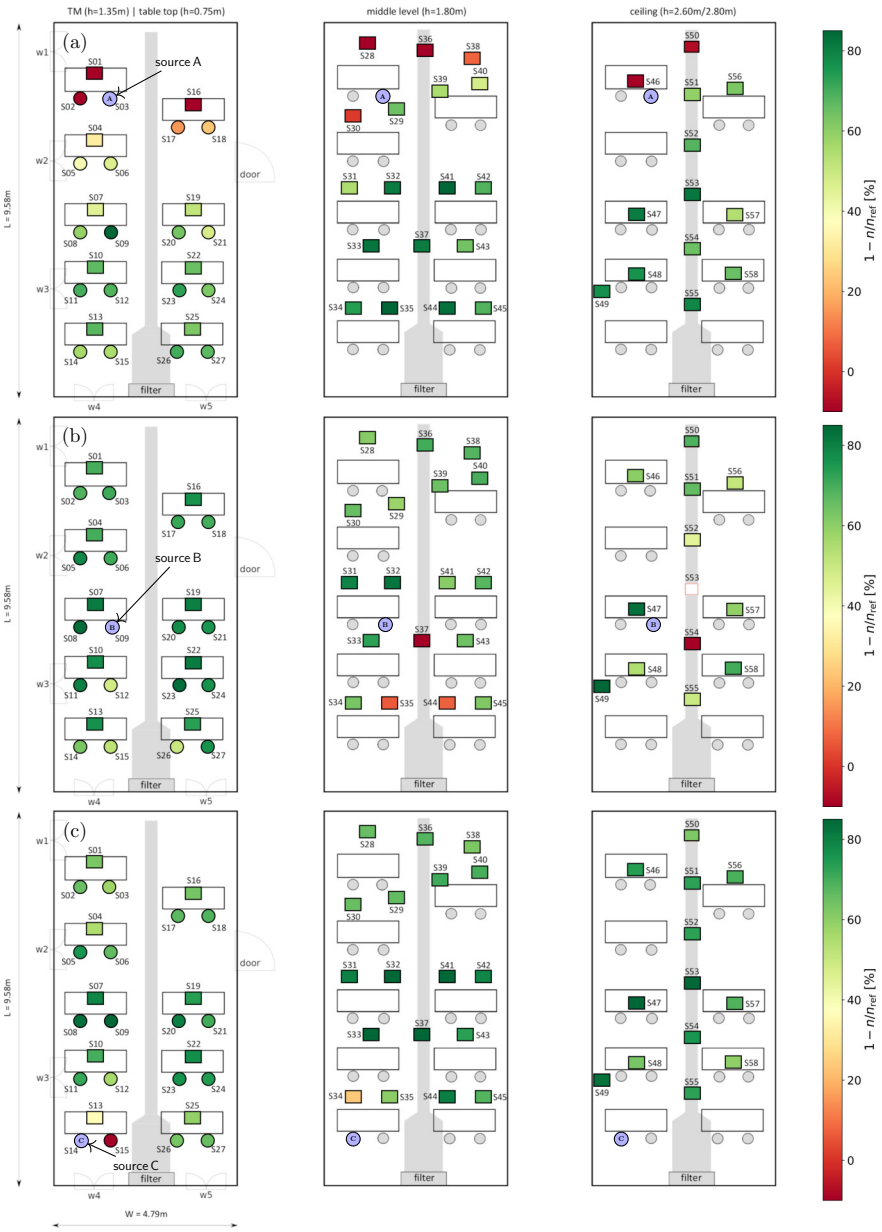

Figure 11: Time-averaged and normalised concentration $1 - n/n_{\mathsf{ref}}$ for interval A in case of LMV : (a) source A, (b) source B and (c) source C.

case. The spatial-averaged concentration for source A is 50.6%, for source B 62.1% and C the concentration 57.9% lower. Moreover, significant differences in the concentration distribution depending on the source position are found. For the measurements with the source at position A in the rear part of the room, a lower concentration of $42\% < 1 - n/n_{\mathsf{ref}} < 98\%$ is obtained compared to the reference case, while in the front half it is $1 - n/n_{\mathsf{ref}} < 40\%$. Moreover, as well sensor positions with higher concentrations compared to the reference case are found. Here elevated concentrations are detected for positions $S01$ of 15.0%, $S02$ of 18.1%, $S16$ of 5.9%, $S36$ of 55.2% and $S50$ of even 76.5%.

The elevated particle concentration in the front area of the room uncovers two issues of the ventilation system in this particular arrangement. Firstly, for all three source positions, the exhaled particles are deflected in the direction of the aisle, since the extraction tube is mounted there on the ceiling. As a consequence, higher concentrations are found at sensor position $S36$ and $S50$ for source A, $S37$ and $S54$ for source B and $S15$ for source C. Secondly, for source A two effects lead to elevated concentrations in the front area in relation to the rear half of the room. Due to the pressure drop for the extraction tube in longitudinal direction, the suction is no longer as strong at the end of the tube and thus a lower extraction rate obtained at the front of the room. In addition, the filtered air which enters the room on floor level and flows from back to front mixes with the existing air in the room and additionally rises due to buoyancy. These two effects lead to a higher concentration in the front half of the test environment. However, generally, the measurement results show that the particle concentration is significantly lower at almost each sensor position.

During interval B and C, the ventilation leads to a homogeneous distribution as well as to a continuous decrease of the aerosol concentration. The spatial distribution of the time-averaged concentrations for these two periods are depicted in figure 12 for source position A. The data reveal a homogeneous distribution as well as significant lower particle concentrations in comparison to the reference case. In the present paper, only the result for source position A is presented, but comparable results are obtained for the remaining locations source B and source C. For interval B the spatial-averaged concentration in relation to the reference case is 58.3% lower for source A, 72.3% lower for source B and 58.8% lower for source C. It is noticeable that in the case of position source B, which is located in a centre position of the room, the reduction in aerosol concentration is greater than in the two cases with the source in the corners. A detailed discussion on this effect and the dynamics of the particle extraction is given in section 4.2 and section 5. For the interval C the decrease of concentration is almost similar for the three source positions with approximately 96% compared to the corresponding reference case.

Another measurement for LMV was performed in combination with a FFP2 mask. The concentration $1 - n/n_{\mathsf{ref}}$ in case of source B for the interval A is illustrated in figure 13. The spatial distribution of $1 - n/n_{\mathsf{ref}}$ is comparable to the case of LMV without the mask (see figure 11(b)). However, differences can be determined in particular for the middle level at the sensor positions $S37$, $S35$ and $S44$, which are located on the right side of the source directly

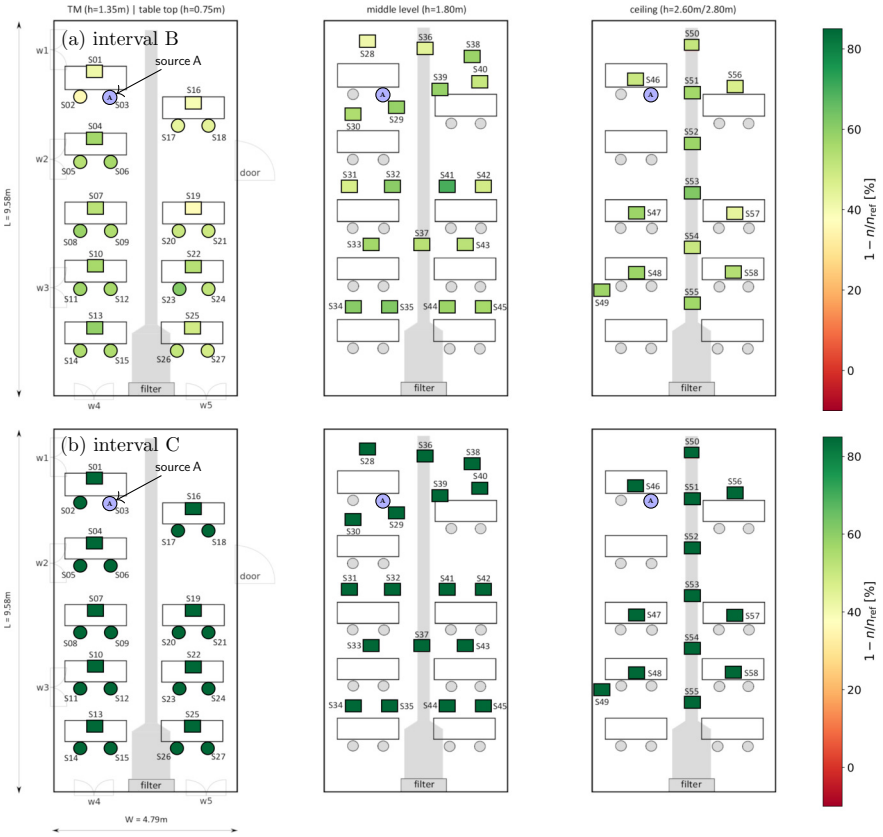

Figure 12: Time-averaged and normalised concentration $1 - n/n_{\mathsf{ref}}$ in percent in case of LMV for source position A: (a) interval B and (b) interval C.

below the extraction tube and just behind on the aisle side. Significantly lower concentrations are found at the mentioned positions for the case with mask, which is due to the fact that the mask restricts the respiratory momentum. The exhaled aerosol is transported towards the ceiling due to the rising air in the vicinity of the TM. In contrast, for the case without the mask, where the exhaling air jet transports the aerosols outside the area in which the buoyancy forces are predominant. As a consequence, the aerosol motion is significantly influenced by the airflow induced by the recirculation system. Here, the mask has a positive effect as it supports the transport of aerosol towards to the ceiling resulting in significant higher concentrations at sensor positions $S46$, $S47$ and $S48$. However, this buoyancy driven transport of the exhaled aerosol toward the ceiling does not lead to a lower concentration on the average. It is found that the spatial-averaged concentration for interval A $\overline{N/N_0} \approx 0.023\%$ is similar for both scenarios, with and without mask. The same result is observed for interval B and C (details see table 1). This result indicates that the mask in the present study does not lead to an additional reduction of the aerosol concentration when

Figure 13: Time-averaged and normalised concentration $1 - n/n_{\mathsf{ref}}$ in percent in case of LMV and FFP2 mask for interval A and source position B.

the ventilation system is active, but to a faster transport to the ceiling area. As a consequence, there is a lower concentration at the lower levels.

4.1.4. Moving body

The influence of moderate movements in the room on the aerosol dynamics is additionally studied. For this purpose, at the beginning of interval B a person walks four times up and down every five minutes. As a result, there is an additional mixing of the air and thus differences in the spatial distribution of the particle concentration compared to the static case. Figure 14 shows the impact of the walking person on the aerosol distribution. It illustrates the changes of the aerosol concentration $1 - n_{\mathsf{mb}}/n_{\mathsf{s}}$ in percent for the scenario with the moving person $n_{\mathsf{mb}} = N_{\mathsf{mb}}/N_0$ in relation to the corresponding static case $n_{\mathsf{s}} = N_{\mathsf{s}}/N_0$ for interval B. Here and in the following the indices mb indicates moving body and s static.

For the reference case, the spatially averaged aerosol concentration for both scenarios, static $\overline{N}_{\mathsf{s}}/N_0 = 0.088(1)\%$ as well as the walking person $\overline{N}_{\mathsf{mb}}/N_0 = 0.087(1)\%$ and the corresponding standard deviation, are similar. However, differences are found for the spatial distribution especially near the source at the sensor positions $S07$ and $S19$ (see figure 14a), representing the sensors on the source's table and the adjacent table to the right. Here, higher concentrations are measured due to the interaction of the exhaling air jet and the moving person, resulting in a wider spreading of the aerosol in front of the source. Further, lower values are obtained in the rear part of the room whereas elevated concentrations occurred in the front part of the test environment. This result shows clearly that even a minor movement significantly influence the spatial distribution of the aerosol concentration significantly.

For the interval B, in case of LMV, the spatially averaged concentration $\overline{N}_{\mathsf{mb}}/N_0 = 0.0257(54)\%$ is significantly lower compared to the reference case,

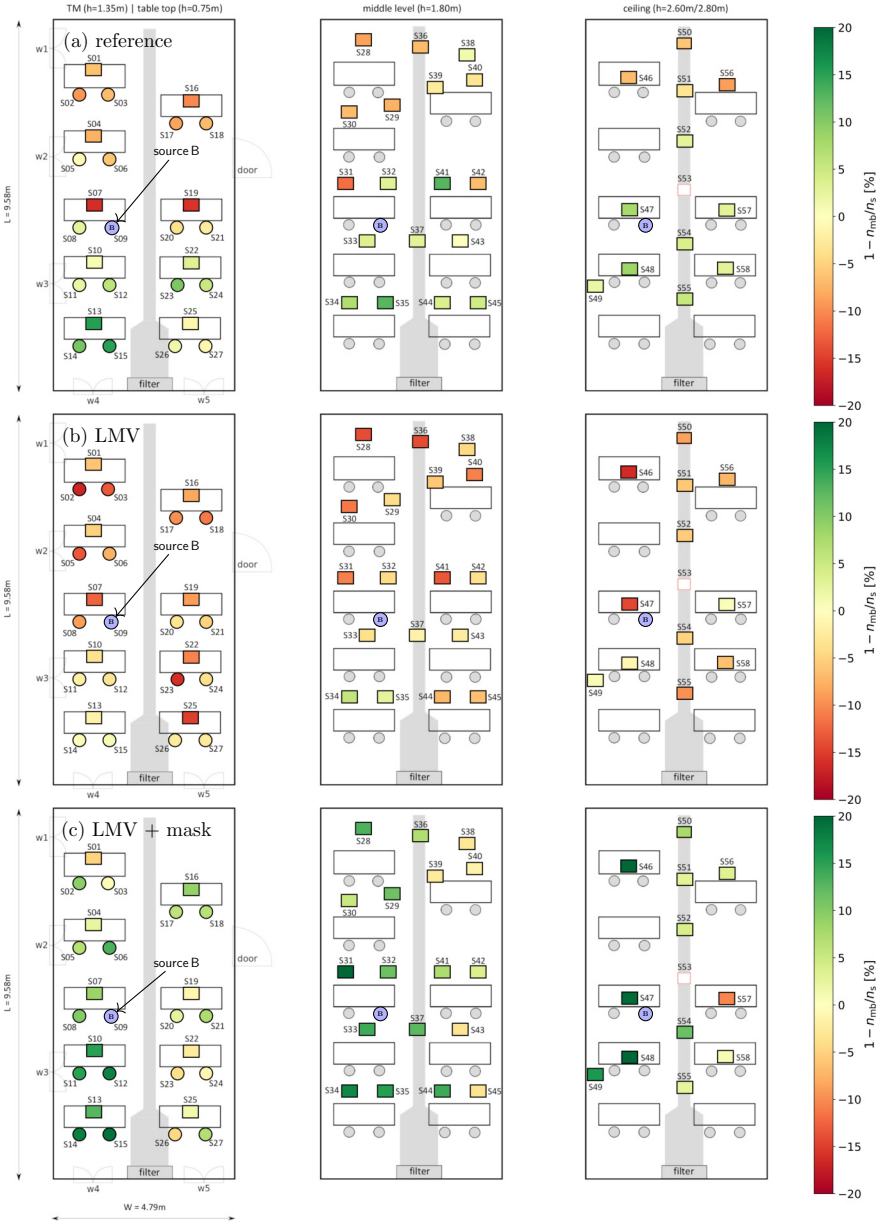

Figure 14: Time-averaged and normalised concentration $1 - n_{\mathsf{mb}}/n_{\mathsf{s}}$ in percent for interval B and source position B. (a) reference case, (b) LMV and (c) LMV and mask.

however, 6% higher than the static case. Furthermore, elevated concentration are found for almost all sensors and not only for individual positions. This increase is a direct consequence of the interaction of the airflow towards the extraction tube with the person walking in the aisle. In the process, the moving person encounters the exhaled air stream flowing in direction of the tube at the ceiling. Especially to the right of the source, where significantly higher aerosol concentrations are noted for the static case (see sensor positions $S37$ and $S54$ in figure 11b). In this case, the disturbance of the airflow leads to a mixing of the aerosol due to the trailing vortex induced by the person walking up and down. Consequently, fewer particles reach the ceiling area where they are extracted and thus higher concentrations are found for almost all sensor positions. Even though the increase in the mean concentration is low at 6%, the results reveal an effect for such LMV-systems. Further, higher dynamics can result in a breakdown of a stable airflow in direction of the air extraction which in turn can lead to a higher particle concentration in the room.

In the case of LMV with mask (fig. 14c) the spatially averaged concentration is $\overline{N}_{\mathsf{mb}}/N_0 = 0.0222(5)\%$ for the moving body scenario which is 9% lower compared to the static case. It is difficult to find a clear explanation for the lower concentration. An obvious reason is the fact that the mask does not fit equally well in every measurement, which results in a varying amount of aerosol passing the mask due to leakage. Another explanation is that in the cases with a mask, there is no exhaling air jet in direction of the aisle. Here, the aerosol rises near the body towards the ceiling. As a result, there is less aerosol in the aisle area which can interact with the person walking through, leading to increased mixing. This thesis is supported by the fact that in the static case at sensor position $S37$, in the corridor to the right of the source, at a height of $h = 1.80\,\mathrm{m}$, the concentration is not increased in contrast to the case with ventilation and without mask. Furthermore, the moving body may create a flow below the extraction tube, which could lead to an enhanced transport of aerosols towards the extraction tube. These are three possible explanations that need to be verified in further studies.

4.2. Aerosol dynamics

In addition to the spatial distribution, the time series of the aerosol concentration is analyzed with respect to the removal factor Γ_i/ACP, the fluctuations $\sigma(\tau)/\tau$ and the aerosol flow rate $\Delta N/\mathsf{ACP}$. The definitions of these parameters are found at the beginning of the result section (sec. 4).

The discussion on the aerosol dynamics starts with the analysis of the LMV's removal rate. Figure 15 shows the removal factor Γ/ACP as a function of the source position. Here, Γ/ACP is a measure how many ACs are needed to reduce the aerosol concentration from the maximum peak $\overline{N}_{\mathsf{max}}$ to a local concentration of $0.2\,\overline{N}_{\mathsf{max}}$. The illustration clearly reveals that $\Gamma/\mathsf{ACP} < 2.0$ at almost every sensor position. The average over all sensors $\overline{\Gamma}/\mathsf{ACP}$ is for source A 1.07(17), for source B 1.11(7) and for source C 0.89(6). This means that on the average an $AC \leq 1.11$ is needed to reduce the aerosol concentration from the average maximum to 20% of this maximum. However, elevated Γ/ACP are found near

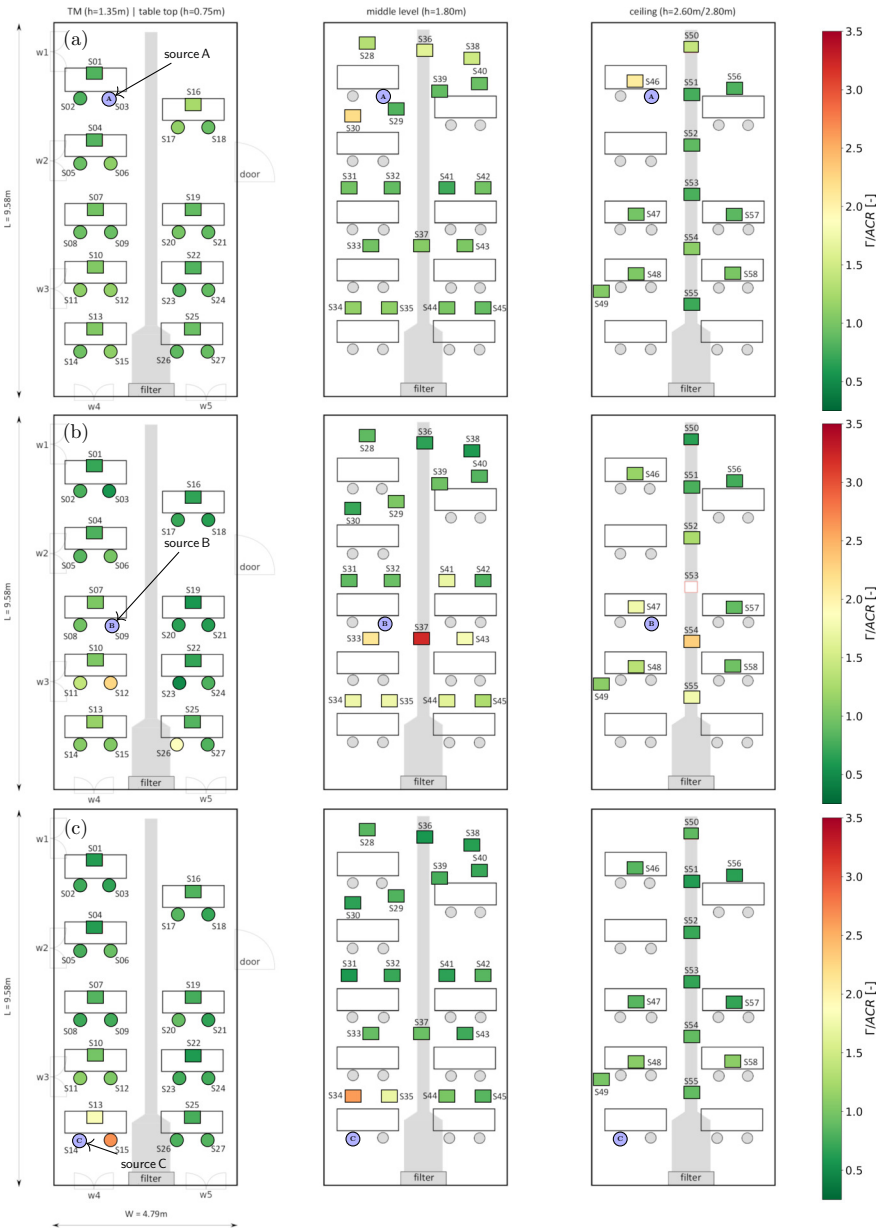

Figure 15: Aerosol removal factor Γ/ACP in case of LMV for the three source positions: (a) source A, (b) source B and (c) source C

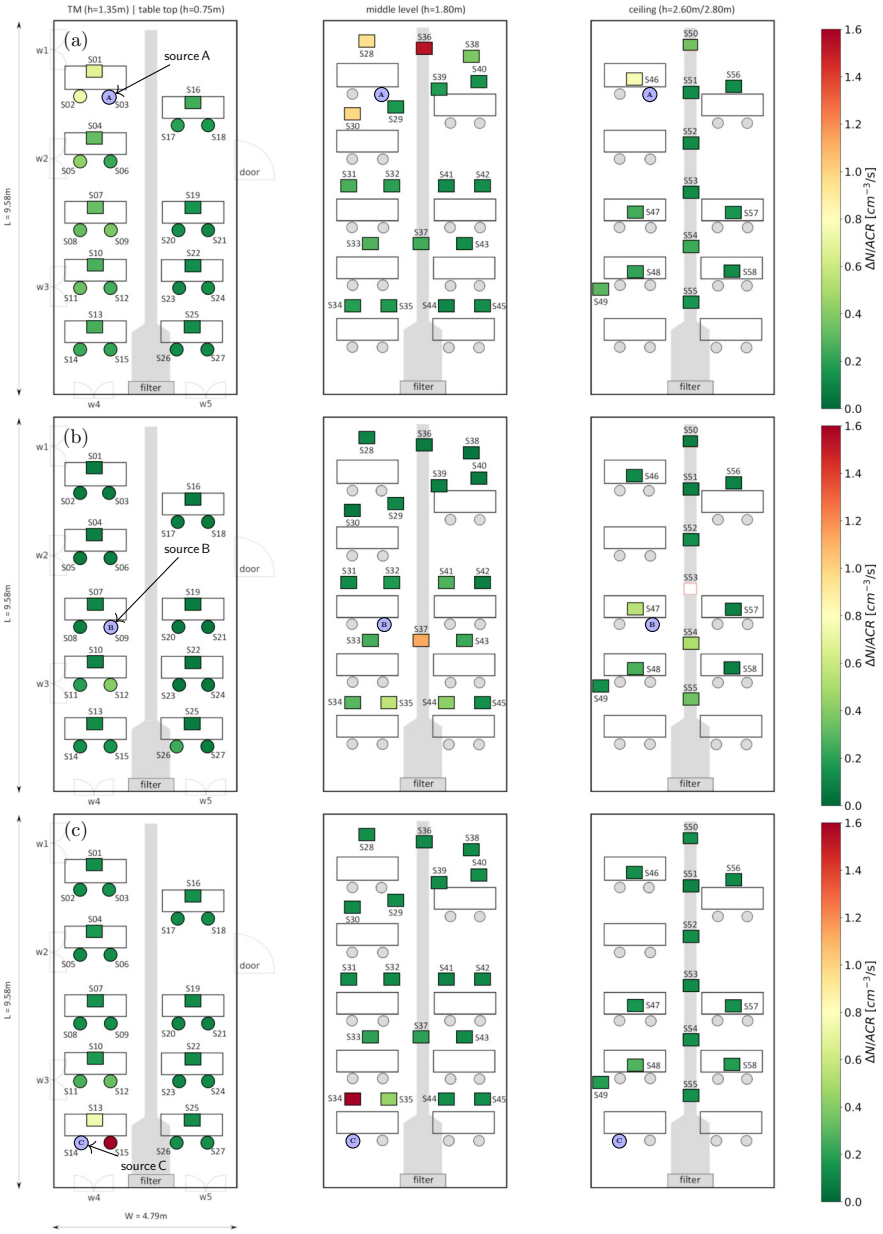

Figure 16: Aerosol flow $\Delta N/ACP$ in case of LMV for the three source positions: (a) source A, (b) source B and (c) source C.

the source and here in particular for sensors mounted at a height of $h = 1.80\,\mathrm{m}$ and at ceiling level. The reason for that increased removal factor is, that a larger amount of the aerosol rises due to buoyancy and accumulates under the ceiling, which leads to a higher concentration there and thus to a higher removal factor in contrast to the other sensor positions. This result underlines the strong impact of buoyancy in the vicinity of a human body and the need to take this effect into account when developing and designing a ventilation concept. Additionally, a comparison of the removal rate for the different source position reveals significant differences between the case for source B (fig. 15b) in the centre of the room for source A (fig. 15a) as well as for source C (fig. 15c) in the corner positions. For the corners higher removal factors are calculated over a larger area behind the source B. The reason for this effect cannot be clearly identified from the available data. However, it is reasonable to assume that this is due to the interaction of the inlet air introduced at floor level, which then rises slowly due to the suction at the ceiling area and the buoyancy flows induced by the heat loads. As a result, the flow of the aerosols in the direction of the extraction tube is limited. In contrast, the influence of the supply air is not as strong or barely present in the front and rear corner of the room. Therefore, increased Γ/ACP is found near the source positions A and C in the corners.

An additional important information is where an increased flow of aerosol is present. Figure 16 depicts the spatial distribution of the aerosol flow rate $\Delta N/\mathsf{ACP}$ for the three different aerosol source positions. For all cases, $\Delta N/\mathsf{ACP}$ is lower than $0.25\,\mathrm{cm^{-3}/s}$ at almost each sensor position. On the average $\Delta N/\mathsf{ACP}$ amounts to $0.28(5)\,\mathrm{cm^{-3}/s}$ for source A, $0.16(1)\,\mathrm{cm^{-3}/s}$ for source B and $0.27(2)\,\mathrm{cm^{-3}/s}$ for source C. In particular for source B (fig. 16b) a homogeneous distributed and controlled transport towards the extraction tube is found. Here, only at the middle level right to the exhaling TM ($S37$) a significant higher flow of $\Delta N/\mathsf{ACP} = 1.13\,\mathrm{cm^{-3}/s}$ is found. An almost comparable behaviour is found as well for source A (fig. 16a) and source C (fig. 16c) for the most sensor positions, except in the vicinity of the exhaling TM. The finding indicates that due to the controlled suction of the aerosols at the ceiling no significant cross-flow is developed, which would lead to an uncontrolled spreading of aerosol in the room.

For the two source positions in the corner, however, significant higher aerosol flow rates are found in the vicinity of the exhaling TM. In case of exhaling at source A, an increased flow of $\Delta N/\mathsf{ACP} = 1.54\,\mathrm{cm^{-3}/s}$ is detected at the middle level for position $S36$. For source C, a strongly increased aerosol flow rate of $\Delta N/\mathsf{ACP} = 4.94\,\mathrm{cm^{-3}/s}$ and $\Delta N/\mathsf{ACP} = 1.97\,\mathrm{cm^{-3}/s}$ is found for sensors mounted at the TM's face to the right ($S15$) and at the middle level directly in front of the exhaling TM ($S34$). The very high flow rate at $S15$ is due to the fact that there is the aerosol source out of reach of the extraction tube and thus there is an uncontrolled airflow, which leads to a higher aerosol flow rate at this position. The finding reveals the stringent necessity of a controlled flow in rooms and buildings to reduce the aerosol concentration on height levels where other persons inhale possible virus loaded aerosol. Although an increased aerosol flow is found for the corners, due to the controlled extraction of the aerosol at the

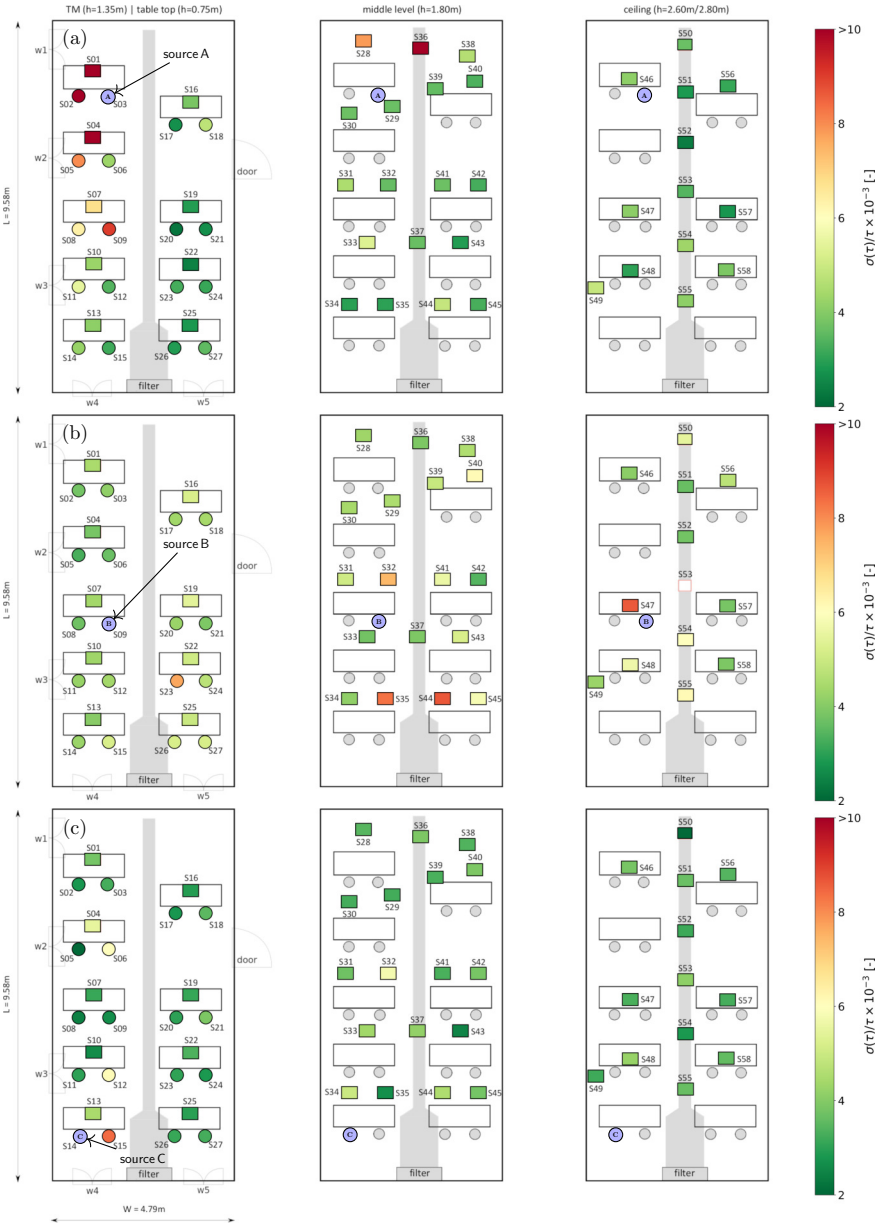

Figure 17: Fluctuations $\sigma(\tau)/\tau$ in case of LMV for the three source positions: (a) source A, (b) source B and (c) source C.

595 ceiling, a lower aerosol flow for most positions in the room is detected.

Beside the removal and flow rate of the aerosol, the stability of transport towards the extraction tube at the ceiling is an additional factor of interest. Figure 17 depicts $\sigma(\tau)/\tau$ for the three aerosol source positions. In case of source

A (fig. 17a) increased fluctuations are found in the vicinity of the exhaling TM at the lower level for the sensors $S01$, $S02$ and $S04$ as well as at middle level for sensor $S36$ with $\sigma(\tau)/\tau$ up to 15.4×10^{-3}. Further elevated fluctuations are also found at the two tables right behind. However, for source B (fig. 17b) and source C (fig. 17c) increased $\sigma(\tau)/\tau$ are just found in the vicinity of the exhaling TM. Moreover, here $\sigma(\tau)/\tau$ is significantly lower and the region where elevated values are found is smaller in comparison with source A. The explanation that the aerosol transport towards the extraction tube at the ceiling is such stronger disturbed for source position A is twofold. Due to the pressure drop over the length of the extraction tube, the suction at the end is not that efficient like at the beginning or at the half length of the tube. As a result, any disturbance has a much stronger impact on the aerosol transport. In particular, the fluctuations of the predominant buoyancy flow there has an strong impact on the stability. As a result, the exhaled aerosol is transported towards the ceiling and mixes with the room air, which leads to an increased aerosol concentration in the area above the TM like illustrated in figure 11a.

In case of the exhaling TM at the position B, stronger fluctuations are found just at the ceiling right above the TM ($S47$), at the middle level($S32$) as well as to the left ($S35$) and to the right ($S44$) of the outlet where the filtered air enters the room. The increased fluctuations at the ceiling is caused by the rising warm air emitted from the TM. Regarding the higher fluctuations near the air outlet it seems that the out-flowing air induces additional turbulences, which influences the aerosol transport. However, the reason why that higher fluctuations are just present in case of source B is not clear and possible the result of an individual flow situation. For the source C increased dynamics are found for the position to the right of the exhaling TM ($S15$). Here is the aerosol source in the right rear corner behind the beginning of the extraction tube and near to the air outlet. Since the source is located outside the direct influence of the extraction tube, the flow is determined by the buoyancy flow induced by the TM and the forced flow from the outlet, leading to higher fluctuations at sensor position $S15$.

In addition, the impact of a mask and a moving body on the aerosol dynamics is analysed. Figure 18 shows the results for an exhaling TM with mask at position source B regarding the removal factor and the aerosol flux. On the average a significant lower removal factor is found for the case with mask (fig. 18(a)) in comparison with the corresponding case without a mask (fig. 15(b)). For the exhaling TM with mask the mean removal factor is $\overline{\Gamma}/\mathsf{ACP} = 0.92$ and for the case without mask $\overline{\Gamma}/\mathsf{ACP} = 1.10$. This means, that for the scenario with mask the aerosol removal factor is $0.17 \times ACP$ higher. In particular behind and to the right of the exhaling TM a significant shorter aerosol removal time is detected. For this area the removal is from $0.21 \times ACP$ up to $0.49 \times ACP$ faster, except at the measurement position directly behind the TM at the middle level ($S33$). At position S33 a $0.42 \times ACP$ slower removal rate is found. This, in general, faster aerosol removal rate in the vicinity of the exhaling TM results from the fact that a lower exhaling momentum is achieved by the mask. As a result, the predominant buoyancy flow transports the aerosols directly towards the ceiling. In contrast to the case without mask where the exhaling air jet

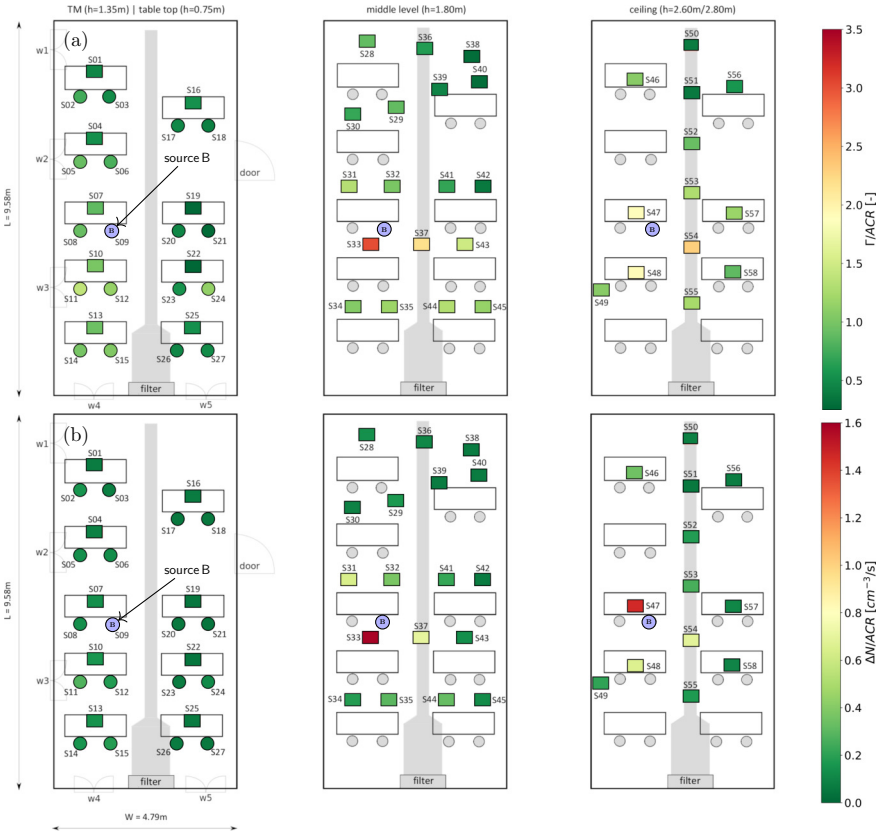

Figure 18: Aerosol dynamics for source B in case of the mask scenario: (a) removal factor Γ/ACP and (b) aerosol flow $\Delta N/\mathsf{ACP}$.

leads to an increased spreading of the aerosol further away from the TM and thus also into an area in which the buoyancy forces are no longer predominant.

The results of the aerosol flow $\Delta N/\Gamma$ (Fig. 18) also confirm the previously described finding. For the mask scenario a strongly increased aerosol flow is found in the vicinity of the exhaling TM at the middle level and at the ceiling. While the aerosol flow is on the average $\overline{\Delta N}/\mathsf{ACP} = 0.22(4)\,\mathrm{cm}^{-3}/\mathrm{s}$, a significantly higher value of up to $\overline{\Delta N}/\mathsf{ACP} = 1.58\,\mathrm{cm}^{-3}/\mathrm{s}$ is determined directly above the TM at sensor position $S33$ and $S47$. Moreover, a comparison with the results for the scenario without a mask (fig. 16b) also discloses the impact of the mask on the aerosol flow. At the sensor positions $S33$ and $S47$ above the exhaling TM $\overline{\Delta N}/\mathsf{ACP}$ is 6.3 and 2.7 times higher in case of wearing a mask, respectively.

At last, the impact of a moving body on the aerosol dynamics is discussed. For the removal factor Γ/ACP and the aerosol flow $\Delta N/ACP$ no significant influence is found in comparison with the static case (not shown here). However, significant influences are found for the fluctuations. Figure 19 shows

Figure 19: Fluctuations $\sigma(\tau)/\tau$ in case of moving body scenario for source B.

the corresponding fluctuations $\sigma(\tau)/\tau$ in case of the moving body. On average, the fluctuations for the static and the moving body case are similar with a value of $\sigma(\tau)/\tau = 4.9 \times 10^{-3}$. However, the range of fluctuations for the moving body case is larger and the spatial distribution differs. The values ranging from $3.3 \times 10^{-3} \leq \sigma(\tau)/\tau \leq 8.9 \times 10^{-3}$ for the static case and $2.55 \times 10^{-3} \leq \sigma(\tau)/\tau \leq 1.97 \times 10^{-2}$ for the moving body case, respectively. In particular the maximum fluctuations are four times higher in case of the moving body, however, elevated values are found only at individual positions on the two higher measurement levels. For the lower level (TM face and table) the spatial distribution is almost similar. Of course, the impact of additional movements in rooms depends strongly on the nature and strength of motion as well as on the flow conditions in the room itself. But, in general, it seems that moderate movements do not lead to an interruption of the aerosol extraction and still a controlled aerosol flow towards the extraction tube at the ceiling is ensured.

4.3. Discussion

Figure 20 shows the spatial mean of the time-averaged normalised number concentration $\overline{N}/N_0$ as a function of the scenario and interval. The charts for the corresponding intervals are colour-coded. In addition, table 1 lists the temporal and spatial averaged values for $\overline{N}/N_0$ and $1 - \overline{n}/\overline{n}_{\mathsf{ref}}$ as well as the corresponding standard deviations, respectively as a function of the interval. In general, the mean aerosol concentration for all cases without a control strategy are comparable, except source C for interval A, where a lower concentration is found. The reason for this decreased concentration is that less sensors are installed near the source C, compared to the other two source positions. Hence, the aerosol concentration at this position is underestimated. However, at the end of the total measurement time all source positions have a similar concentration of $\overline{N}/N_0 \approx 0.07\%$, which means that 19.5% of the exhaled aerosol are still in the air. Moreover, the aerosol is homogeneously distributed indicated by the low standard deviation of approximately $0.07 \times \overline{N}$. This result shows that for the

scenario / interval	$\overline{N}/N_0$ [%]			$\sigma(N)/\overline{N}$ [%]			$1-\overline{n}/\overline{n}_{\mathsf{ref}}$ [%]			$\frac{\sigma(1-n/n_{\mathsf{ref}})}{1-\overline{n}/\overline{n}_{\mathsf{ref}}}$ [%]		
	A	B	C	A	B	C	A	B	C	A	B	C
reference (A)	0.055	0.094	0.072	58	15	7	-	-	-	-	-	-
reference (B)	0.058	0.088	0.073	55	16	6	-	-	-	-	-	-
reference (C)	0.038	0.080	0.071	88	29	7	-	-	-	-	-	-
mask (B)	0.042	0.069	0.057	77	17	7	31	22	21	66	23	8.0
OWV (B)	-	0.041	0.027	-	16	14	-	52	67	-	9.6	7.6
LMV (A)	0.027	0.039	0.002	76	23	22	51	58	97	57	14	0.5
LMV (B)	0.023	0.024	0.004	111	22	29	62	72	95	39	5.9	0.5
LMV (C)	0.016	0.033	0.004	79	23	24	58	59	97	55	18	0.6
LMV/mask (B)	0.023	0.024	0.003	79	23	24	58	59	96	32	3.5	0.9
LMV/MB (B)	0.027	0.026	0.002	107	21	17	59	71	97	56	6.9	0.6
LMV/MB/mask (B)	0.020	0.022	0.002	84	23	20	66	75	97	34	5.7	0.6

Table 1: Averaged normalised particle density $\overline{N}/N_0$ and $1-\overline{n}/\overline{n}_{\mathsf{ref}}$ and the corresponding standard deviation σ for the intervals A, B and C (in brackets after the scenario identifier).

present configuration the aerosol spreads throughout the room within a time span of less then 2400 s due to the thermal convective airflow, induced by the TM. This finding emphasises the vital necessity of control strategies to reduce the aerosol concentration in rooms.

An increased concentration is also found in case of the mask scenario, where 15.4% of the exhaled aerosols are still in the air at the end of the total measurement time. It reveals that a reduction of the aerosols in a room by means of a FFP2/KN95 mask is restricted. This limitation of mask use against respiratory virus transmission is reported in other studies Jefferson et al. (2009); Bin-Reza et al. (2012); Aggarwal et al. (2020); Long et al. (2020) as well. In particular, if a mask is not tightly sealed to the skin, a leakage flow occurres, especially during exhaling, when there is an overpressure under the mask. Nevertheless, FFP2/KN95, FFP3/KN99 as well as home made masks have an self-protective effect of uninfected persons, since masks effectively filter virus-loaded particles Belkin (1997); Davies et al. (2013); Brainard et al. (2020). Moreover, it is almost uncontroversial that a widespread use of face masks in an epidemic reduces the contagiousness by respiratory virus transmission Mitze et al. (2020). All in all mask use is an important component in a holistic control strategy, however, it is limited regarding an aerosol reduction.

Significant lower particle concentration is detected for the interval C in the cases with active ventilation. For OWV 7.3% and for all LVM scenarios (including mask and moving body) approximately 1% of the exhaled aerosols are active in air at the end of total measurement time. That means in case of LVM all particles are removed after a period of approximately 1800 s. Moreover, as well for interval A and B a much lower concentration $\overline{N}/N_0$ is found for the scenarios with a control strategy in comparison to the corresponding reference cases. In particular for the interval B, in which the aerosol concentration has its maximum, all here tested control strategies lead to significant lower concentrations. However, there are clear differences in terms of effectiveness between the control strategies regarding removal efficiency, spatial distribution and dynamics, which is summarised in the following.

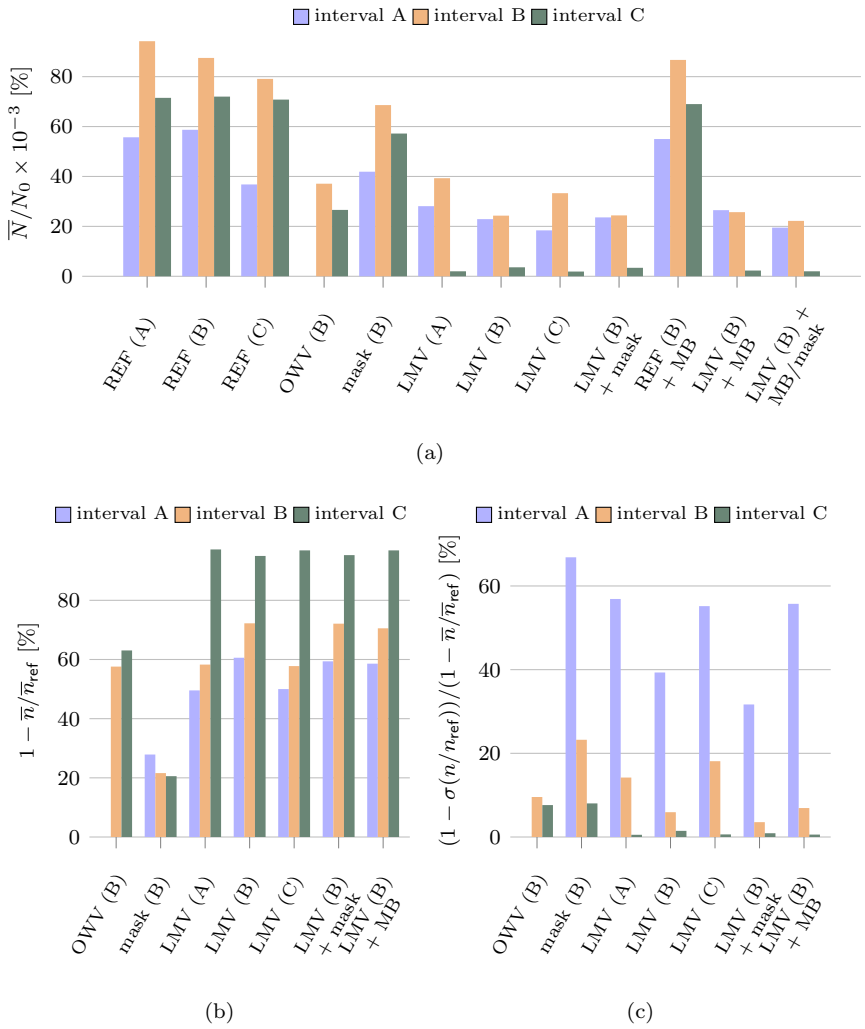

Figure 20: (a) Overview of the aerosol concentration $\overline{N}/N_0$ for the respective configurations and intervals. (b) Reduction efficiency $1-\overline{n}/\overline{n}_{\mathsf{ref}}$ and (c) the corresponding standard deviation σ. The letters in brackets after the scenario identifier denotes the source position.

An overview of the particle removal-efficiency is given in figure 20b. It shows the temporal and spatial averaged $1-n/n_{\mathsf{ref}}$ as a function of the control strategy. The LMV-system with air purifier provides an efficient aerosol removal for the exhale (interval A) and for the decay period (interval B). In case of interval A and B a decrease of aerosol concentration compared to the corresponding reference case of $51\% \leq 1-n/n_{\mathsf{ref}} \leq 62\%$ and $58\% \leq 1-n/n_{\mathsf{ref}} \leq 72\%$ is found, respectively. At the end of the measurement time the decrease of the aerosol concentration is more then 95%. An efficient aerosol reduction is obtained in

case of OWV ($1 - n/n_{\mathsf{ref}} = 52\%$) for interval B as well. However, it should be noted that for OWV the effectiveness depends on the outdoor conditions like air temperature, air humidity or the wind speed. Consequently, a reliable, stable and controlled ventilation by means of OWV is not guaranteed. Nevertheless, for outdoor conditions, as prevailed during our measurement, the OWV is efficient to reduce the aerosol concentration in a room significantly. In contrast, for the only mask scenario the reduction of the aerosol concentration was much less effective in comparison to LMV and OWV. For this scenario, the decrease is only 31% for interval A, 22% for interval B and 21% for interval C.

In addition, figure 20c shows the normalised standard deviation for the spatial mean. Here, the highest standard deviation is found for mask only and the lowest standard deviation for the scenario LMV in combination with a mask. The increased standard deviation in the mask only case is the result of the turbulent buoyancy flow near the source TM. This leads to higher fluctuations at the ceiling level directly above the source TM as well as for individual positions at the middle level behind the source. Further, significant differences are identified for the individual LVM scenarios. A comparison as a function of the source position reveals that for the corner source-positions (source A and source C) the standard deviation is approximately 30% higher compared to position source B, which is located in the centre of the room. This result clearly shows that the aerosol removal as well the spatial distribution depends on the source position. In addition, it is found that in case of the moving body scenario the particle density is more inhomogeneously distributed compared to the corresponding static case.

The main results of the aerosol dynamics in case of LMV are summarised in figure 21. It illustrates the spatial average as well as the corresponding minimum and maximum of: (21a) the removal rate Γ/ACP, (21b) the flow rate $\Delta N/\mathsf{ACP}$ and (21c) the fluctuations σ_τ/τ. It is found that the mean removal rate Γ/ACP is comparable for all scenarios and it amounts $\Gamma/\mathsf{ACP} = 1.00(8)$. This means that on the average 1 air-exchange is needed to reduce the aerosol concentration from its local maximum to a concentration of $0.2\times\overline{N}_{\mathsf{max}}$. However, at some individual positions air exchanges up to 3.6 are obtained. These positions with elevated $\Delta N/\mathsf{ACP}$ depend strongly on the source position. Increased air exchange rates are found: for source A on the middle level to the left behind and on the ceiling level directly above the exhaling TM, for source B on the ceiling level directly above and on the middle level to the right of the source and for source C on the lower level right to and on the middle level in front of the source. Furthermore, in the configuration tested here the mask has a small impact on the mean removal rate. In the case of source B, Γ/ACP is 0.19 lower for the scenario of LMV with mask in comparison with the corresponding case without mask. Moreover, as well the maximum and the minimum of Γ/ACP is slightly lower in the case with mask. This lower Γ/ACP is due to the fact that the mask supports the transports of aerosols towards the extraction tube, which has been explained in detail in the result section (sec. 4.2) before. A comparable result is also found for the moving body scenario.

The mean aerosol flow rate (fig. 21b) is for source B almost compara-

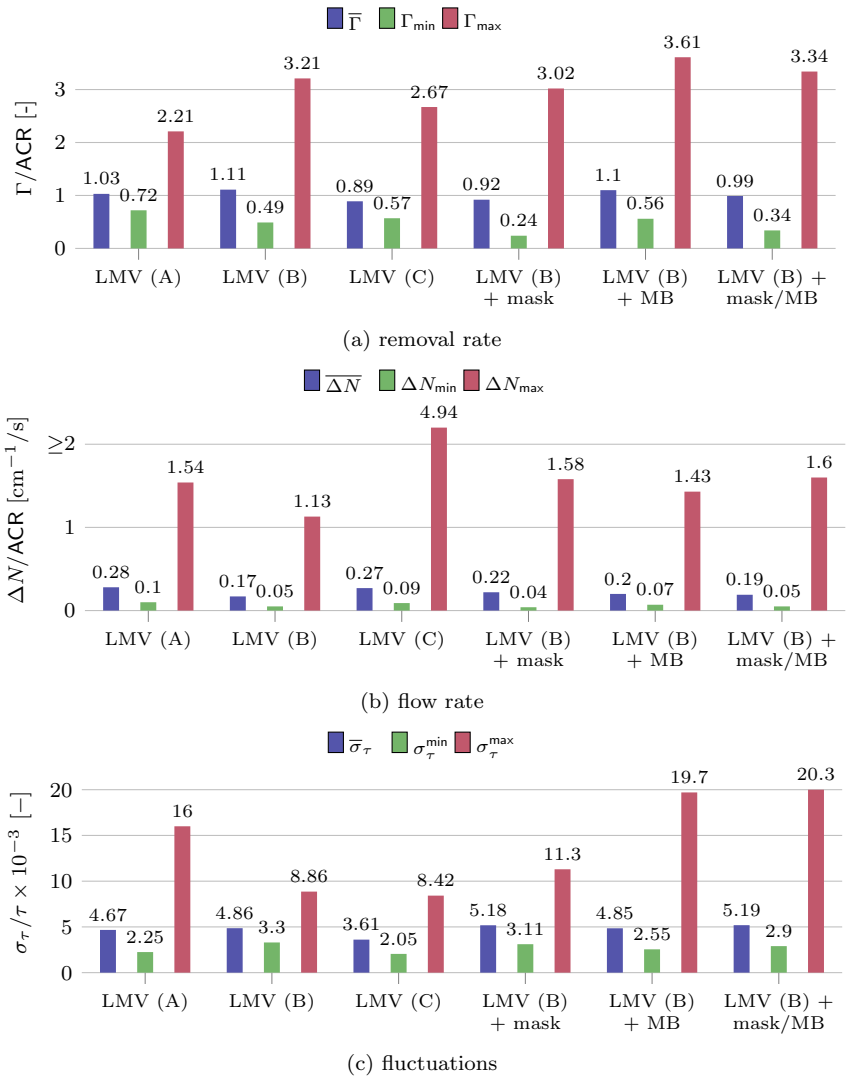

Figure 21: The spatial average as well as the minimum and maximum values for: (a) normalised aerosol removal rate Γ/ACP, (b) aerosol flow rate $\Delta N/\mathsf{ACP}$ and (c) normalised fluctuations σ_τ/τ. The letters in brackets after the scenario identifier denotes the source position.

ble for all scenarios and the amount on the averaged over all scenarios, is $\Delta N/\mathsf{ACP} = 0.20(2)\,\mathrm{cm}^{-1}/\mathrm{s}$. For the corner positions significant higher rates of $\Delta N_\mathrm{A}/\mathsf{ACP} = 0.28\,\mathrm{cm}^{-1}/\mathrm{s}$ and $\Delta N_\mathrm{C}/\mathsf{ACP} = 0.27\,\mathrm{cm}^{-1}/\mathrm{s}$ are found. In addition, for all scenarios significantly higher flow rates are found at individual positions in the vicinity of the source (see fig. 16). In particular, in the case of source C a very high change rate of $\Delta N/\mathsf{ACP} > 3.6$ is found directly in font

and right to the source, while for all other scenarios the maximum is always $\Delta N/\mathsf{ACP} \leq 1.6$. As already analysed in section 4.2 this effect is due to the fact that the source is outside the direct sphere of influence of the extraction tube. Regarding, the impact of mask and MB in case of LMV at source position B, slightly higher mean flow rates are found as well as higher maximum flow rates for individual positions compared to LMV (B).

An overview of the results for the fluctuations are summarised in figure 21c. The figure shows the mean as well as the minimum and maximum fluctuations in function of the LMV scenario. The mean fluctuations is almost similar for all scenarios, except for LMV at source position C. Here significant lower fluctuations are detected. This lower fluctuations are due to the fact that there is less interaction with the air flow in the room, as the source is outside the direct influence of the extraction tube. Additionally, significant higher fluctuations are found at individual positions for LMV source A and the two MB scenarios. In the case of MB the increased fluctuations are a direct of result the walking person. The reason of the higher fluctuations for LMV source A, however, is due to the fact that suction at the end of the tube is not strong enough to provide a stable air flow towards the extraction tube at the ceiling. Hence, the buoyancy flow resulting from the TMs are predominant and that leads to an increase of turbulence. Thus higher fluctuations of the aerosol concentration are measured near the source A.

5. Summary and conclusions

The indoor aerosol-dynamics for a configuration representing a class or a conference room situation are investigated. With the objective to verify the spreading and dynamics of an aerosol exhaled from a possible infected person, dispersed artificial saliva is emitted from a single source. In the following the time series of the aerosol concentration is determined by means of more than 60 particulate matter sensors which are installed in the room on three different height levels. Based on the time series the spatial distribution as well as the dynamics of the aerosol transport in the room are characterised and analysed. In the following the most important results are summarised and the consequences are discussed. Subsequently, an overview on the advantages and disadvantages of a LMV-system with air purifier is presented.

For the here investigated test room the most important results are as followed:

1. If there are no counter measures or control methods applied, aerosol spreads throughout the room. Finally, a homogeneous distribution of the saliva particles is obtained, which can be stable for hours and is independently from the source position of the exhaling TM. This finding underlines the need of control methods in order to avoid an uncontrolled spreading of possible virus loaded particles in a room
2. Any here examined counter measures like LMV, OWV and mask results in a significant lower particle concentration. Whereas, in this configuration

the active ventilation concepts LMV and OMV are more efficient compared to the mask.

3. The buoyancy flow from the TM heat release results in a rising of the aerosol in the vicinity of the exhaling TM. Here, higher particle concentrations are found on the higher measurement levels ($h = 1.80\,\mathrm{m}$ and at the ceiling). As a consequence, the buoyancy flow is a crucial factor for the aerosol dynamics and the corresponding spatial distribution of the particles in a room. In particular, in case of a room with an elevated people-density the buoyancy flow becomes a predominant flow condition due to the heat loads of the human bodies.
4. In case of the LMV-system an almost stable and controlled particle transport in direction to the ceiling is identified. On the average significant lower particle concentrations are found in the room in comparison to the corresponding reference cases without control methods. However, the aerosol dynamics depends strongly on the source position of the exhaling TM. If the source position is in a corner of the room, significant higher particle concentrations are found on the average as well as in the vicinity of the exhaling TM for the exhaling and decay period. In addition, it is found that moderate disturbances of the person walking the aisle up and down does not lead to a break-down of the particle transport in direction to the extraction tube. However, positions of significant higher particle concentration are found here.

The here investigated vertical ventilation concept with air filtering has a potential to reduce the aerosol concentration in a room representing a class- or conference situation during the lesson/meeting. However, it should be remarked that this kind of buoyancy-assisted vertical ventilation needs a sufficiently large temperature gradient between the human body and the surrounding air. In particular, if the air temperature is near the temperature of a human body or the breathing air, there is a risk of a breakdown of a controlled transport of exhaled particles in direction to the extraction tube at the ceiling. Furthermore, in general and in particular for this flow situation it could happen that the filtered air is not homogeneously distributed on the ground. As a consequence, people who are further away from the air outlet are cut off from the filtered air. In addition, there is a danger of a short circuit flow between the air outlet and the extraction tube. To overcome that issue it is advisable to cool down the filtered air which enters the room near the floor with the objective to provide a sufficient large temperature gradient and to ensure the filtered air distributes on ground in order to reach the people who are further away from the air outlet as well. Nevertheless, for the design of a ventilation system, the individual geometrics of a room and boundary conditions have to be taken into account, in order to avoid giving a false impression of security.

Acknowledgement

The authors would like to thank all involved partners for fruitful discussions during the measurements and a smooth cooperation. The credit of the funda-

mental pre work on the aerosol generation, its characterization and the aerosol detection system shall be explicitly announced to Daniel Schiepel, Felix Werner and Konstantin Niehaus from DLR. The critical dialog and proof reading of the complex manuscript was acknowledged to DLR colleagues Daniel Schmeling and Annika Köhne.

Funding

The scientific study was partially funded by the DLR and partially by OHB.

References

Aggarwal, N., Dwarakanathan, V., Gautam, N. et al. (2020). Facemasks for prevention of viral respiratory infections in community settings: A systematic review and meta-analysis. *Indian journal of public health*, *64*, S192–S200. doi:10.4103/ijph.IJPH.

Al Huraimel, K., Alhosani, M., Kunhabdulla, S. et al. (2020). Sars-cov-2 in the environment: Modes of transmission, early detection and potential role of pollutions. *The Science of the total environment*, *744*, 140946. doi:10.1016/j.scitotenv.2020.140946.

Arzneimittel-Codex, D. (2007). Neues rezeptur-formularium (nrf) (in german). *Band I–III. Pharmazeutischen Laboratorium des NRF. Eschborn: Govi-Verlag und Stuttgart: Deutscher Apotheker-Verlag*, .

Atchison, C., Bowman, L. R., Vrinten, C. et al. (2021). Early perceptions and behavioural responses during the covid-19 pandemic: a cross-sectional survey of uk adults. *BMJ open*, *11*, e043577. doi:10.1136/bmjopen-2020-043577.

Azimi, P., Keshavarz, Z., Cedeno Laurent, J. G. et al. (2021). Mechanistic transmission modeling of covid-19 on the diamond princess cruise ship demonstrates the importance of aerosol transmission. *Proceedings of the National Academy of Sciences of the United States of America (2021)*, *118*. doi:10.1073/pnas.2015482118.

Azuma, K., Yanagi, U., Kagi, N. et al. (2020). Environmental factors involved in sars-cov-2 transmission: effect and role of indoor environmental quality in the strategy for covid-19 infection control. *Environmental Health and Preventive Medicine*, *25*, 66. doi:10.1186/s12199-020-00904-2.

Bazant, M. Z., & Bush, J. W. M. (2020). *Beyond Six Feet: A Guideline to Limit Indoor Airborne Transmission of COVID-19*. doi:10.1101/2020.08.26.20182824.

Bazant, M. Z., & Bush, J. W. M. (2021). A guideline to limit indoor airborne transmission of covid-19. *Proceedings of the National Academy of Sciences of the United States of America (2021)*, *118*. doi:10.1073/pnas.2018995118.

Belkin, N. L. (1997). The evolution of the surgical mask: filtering efficiency versus effectiveness. *Infection control and hospital epidemiology*, *18*, 49–57. doi:10.2307/30141964.

Bialek, S., Bowen, V., Chow, N. et al. (2020). Geographic differences in covid-19 cases, deaths, and incidence—united states, february 12–april 7, 2020. *Morbidity and Mortality Weekly Report*, *69*, 465–471.

Bin-Reza, F., Lopez Chavarrias, V., Nicoll, A. et al. (2012). The use of masks and respirators to prevent transmission of influenza: a systematic review of the scientific evidence. *Influenza and other respiratory viruses*, *6*, 257–267. doi:10.1111/j.1750-2659.2011.00307.x.

Bjørn, E., & Nielsen, P. V. (2002). Dispersal of exhaled air and personal exposure in displacement ventilated rooms. *Indoor air*, *12*, 147–164. doi:10.1034/j.1600-0668.2002.08126.x.

Blocken, B., van Druenen, T., Ricci, A. et al. (2021). Ventilation and air cleaning to limit aerosol particle concentrations in a gym during the covid-19 pandemic. *Building and environment*, *193*, 107659. doi:10.1016/j.buildenv.2021.107659.

Brainard, J., Jones, N., Lake, I. et al. (2020). *Facemasks and similar barriers to prevent respiratory illness such as COVID-19: A rapid systematic review: (Preprint)*. doi:10.1101/2020.04.01.20049528.

Brankston, G., Gitterman, L., Hirji, Z. et al. (2007). Transmission of influenza a in human beings. *The Lancet Infectious Diseases*, *7*, 257–265. doi:10.1016/S1473-3099(07)70029-4.

Buonanno, G., Morawska, L., & Stabile, L. (2020). Quantitative assessment of the risk of airborne transmission of sars-cov-2 infection: Prospective and retrospective applications. *Environment international*, *145*, 106112. doi:10.1016/j.envint.2020.106112.

Curtius, J., Granzin, M., & Schrod, J. (2021). Testing mobile air purifiers in a school classroom: Reducing the airborne transmission risk for sars-cov-2. *Aerosol Science and Technology*, *55*, 586–599. doi:10.1080/02786826.2021.1877257.

D'Alessandro, D., Gola, M., Appolloni, L. et al. (2020). Covid-19 and living space challenge. well-being and public health recommendations for a healthy, safe, and sustainable housing. *Acta bio-medica : Atenei Parmensis*, *91*, 61–75. doi:10.23750/abm.v91i9-S.10115.

Davies, A., Thompson, K.-A., Giri, K. et al. (2013). Testing the efficacy of homemade masks: would they protect in an influenza pandemic? *Disaster medicine and public health preparedness*, *7*, 413–418. doi:10.1017/dmp.2013.43.

Duan, T., Jiang, H., Deng, X. et al. (2020). Government intervention, risk perception, and the adoption of protective action recommendations: Evidence from the covid-19 prevention and control experience of china. *International Journal of Environmental Research and Public Health (2020)*, *17*. doi:10.3390/ijerph17103387.

Furuse, Y., Ko, Y. K., Saito, M. et al. (2020). Epidemiology of covid-19 outbreak in japan, from january-march 2020. *Japanese journal of infectious diseases*, *73*, 391–393. doi:10.7883/yoken.JJID.2020.271.

Gaeckle, N. T., Lee, J., Park, Y. et al. (2020). Aerosol generation from the respiratory tract with various modes of oxygen delivery. *American journal of respiratory and critical care medicine*, *202*, 1115–1124. doi:10.1164/rccm.202006-2309OC.

Gupta, J. K., Lin, C.-H., & Chen, Q. (2010). Characterizing exhaled airflow from breathing and talking. *Indoor air*, *20*, 31–39. doi:10.1111/j.1600-0668.2009.00623.x.

Hamner, L. (2020). High sars-cov-2 attack rate following exposure at a choir practice—skagit county, washington, march 2020. *MMWR. Morbidity and mortality weekly report*, *69*.

Howard, J., Huang, A., Li, Z. et al. (2021). An evidence review of face masks against covid-19. *Proceedings of the National Academy of Sciences of the United States of America (2021)*, *118*. doi:10.1073/pnas.2014564118.

Hwang, S. E., Chang, J. H., Oh, B. et al. (2021). Possible aerosol transmission of covid-19 associated with an outbreak in an apartment in seoul, south korea, 2020. *International journal of infectious diseases : IJID : official publication of the International Society for Infectious Diseases*, *104*, 73–76. doi:10.1016/j.ijid.2020.12.035.

Jayaweera, M., Perera, H., Gunawardana, B. et al. (2020). Transmission of covid-19 virus by droplets and aerosols: A critical review on the unresolved dichotomy. *Environmental research*, *188*, 109819. doi:10.1016/j.envres.2020.109819.

Jefferson, T., Del Mar, C., Dooley, L. et al. (2009). Physical interventions to interrupt or reduce the spread of respiratory viruses: systematic review. *BMJ (Clinical research ed.)*, *339*, b3675. doi:10.1136/bmj.b3675.

Johnson, G. R., Morawska, L., Ristovski, Z. D. et al. (2011). Modality of human expired aerosol size distributions. *Journal of Aerosol Science*, *42*, 839–851. doi:10.1016/j.jaerosci.2011.07.009.

Jones, R. M., & Brosseau, L. M. (2015). Aerosol transmission of infectious disease. *Journal of occupational and environmental medicine*, *57*, 501–508. doi:10.1097/JOM.0000000000000448.

Kohanski, M. A., Lo, L. J., & Waring, M. S. (2020). Review of indoor aerosol generation, transport, and control in the context of covid-19. *International forum of allergy & rhinology*, *10*, 1173–1179. doi:10.1002/alr.22661.

Kohl, A., Lange, P., & Schmeling, D. (Eds.) (2021). *Experimental simulation of the human respiration system* volume 22nd STAB/DGLR Symposium on New Results in Numerical and Experimental Fluid Mechanics XIII.

Kolinski, J. M., & Schneider, T. M. (2021). Superspreading events suggest aerosol transmission of sars-cov-2 by accumulation in enclosed spaces. *Physical review. E*, *103*, 033109. doi:10.1103/PhysRevE.103.033109.

Lakdawala, S. S., & Menachery, V. D. (2021). Catch me if you can: Superspreading of covid-19. *Trends in microbiology*, *29*, 919–929. doi:10.1016/j.tim.2021.05.002.

Lange, P., Westhoff, A., Schmeling, D. et al. (2018). Cost-effective human comfort manikin with realistic thermal load for studies of convection-driven ventilation systems. In *Proceedings of Roomvent & Ventilation 2018* (pp. 367–372). SIY Indoor Air Information Oy.

Leung, T. Y. M., Chan, A. Y. L., Chan, E. W. et al. (2020). Short- and potential long-term adverse health outcomes of covid-19: a rapid review. *Emerging microbes & infections*, *9*, 2190–2199. doi:10.1080/22221751.2020.1825914.

Long, Y., Hu, T., Liu, L., Chen, R., Guo, Q., Yang, L., Cheng, Y., Huang, J., & Du, L. (2020). Effectiveness of n95 respirators versus surgical masks against influenza: A systematic review and meta-analysis. *Journal of Evidence-Based Medicine*, *13*, 93–101. doi:10.1111/jebm.12381.

de Man, P., Paltansing, S., Ong, D. S. Y. et al. (2021). Outbreak of coronavirus disease 2019 (covid-19) in a nursing home associated with aerosol transmission as a result of inadequate ventilation. *Clinical infectious diseases : an official publication of the Infectious Diseases Society of America*, *73*, 170–171. doi:10.1093/cid/ciaa1270.

Melikov, A., & Kaczmarczyk, J. (2007). Measurement and prediction of indoor air quality using a breathing thermal manikin. *Indoor air*, *17*, 50–59. doi:10.1111/j.1600-0668.2006.00451.x.

Miller, S. L., Nazaroff, W. W., Jimenez, J. L. et al. (2021). Transmission of sars-cov-2 by inhalation of respiratory aerosol in the skagit valley chorale superspreading event. *Indoor air*, *31*, 314–323. doi:10.1111/ina.12751.

Mittal, R., Ni, R., & Seo, J.-H. (2020). The flow physics of covid-19. *Journal of Fluid Mechanics*, *894*. doi:10.1017/jfm.2020.330.

Mitze, T., Kosfeld, R., Rode, J. et al. (2020). Face masks considerably reduce covid-19 cases in germany. *Proceedings of the National Academy of Sciences of the United States of America*, *117*, 32293–32301. doi:10.1073/pnas.2015954117.

Morawska, L., Johnson, G. R., Ristovski, Z. D. et al. (2009). Size distribution and sites of origin of droplets expelled from the human respiratory tract during expiratory activities. *Journal of Aerosol Science*, *40*, 256–269. doi:10.1016/j.jaerosci.2008.11.002.

Morawska, L., & Milton, D. K. (2020). It is time to address airborne transmission of coronavirus disease 2019 (covid-19). *Clinical infectious diseases : an official publication of the Infectious Diseases Society of America*, *71*, 2311–2313. doi:10.1093/cid/ciaa939.

Morawska, L., Tang, J. W., Bahnfleth, W. et al. (2020). How can airborne transmission of covid-19 indoors be minimised? *Environment international*, *142*, 105832. doi:10.1016/j.envint.2020.105832.

Moritz, S., Gottschick, C., Horn, J. et al. (2021). The risk of indoor sports and culture events for the transmission of covid-19. *Nature communications*, *12*, 5096. doi:10.1038/s41467-021-25317-9.

Nazaroff, W. W. (2016). Indoor bioaerosol dynamics. *Indoor air*, *26*, 61–78. doi:10.1111/ina.12174.

Nishiura, H., Oshitani, H., Kobayashi, T. et al. (2020). *Closed environments facilitate secondary transmission of coronavirus disease 2019 (COVID-19) (Preprint)*. doi:10.1101/2020.02.28.20029272.

Peng, Z., Pineda Rojas, A. L., Kropff, E. et al. (2021). *Practical Indicators for Risk of Airborne Transmission in Shared Indoor Environments and their Application to COVID-19 Outbreaks (Preprint)*. doi:10.1101/2021.04.21.21255898.

Rangel, E. F. (2021). Can climate and environmental factors putatively increase sars-cov2 transmission risks? *American Journal of Biomedical Science & Research*, *11*, 294–299. doi:10.34297/AJBSR.2021.11.001647.

Regli, A., Sommerfield, A., & von Ungern-Sternberg, B. S. (2021). The role of fit testing n95/ffp2/ffp3 masks: a narrative review. *Anaesthesia*, *76*, 91–100. doi:10.1111/anae.15261.

Tang, J. W., Marr, L. C., Li, Y. et al. (2021). Covid-19 has redefined airborne transmission. *BMJ (Clinical research ed.)*, *373*, n913. doi:10.1136/bmj.n913.

Tellier, R. (2009). Aerosol transmission of influenza a virus: a review of new studies. *Journal of the Royal Society, Interface*, *6 Suppl 6*, S783–90. doi:10.1098/rsif.2009.0302.focus.

Tellier, R., Li, Y., Cowling, B. J. et al. (2019). Recognition of aerosol transmission of infectious agents: a commentary. *BMC infectious diseases*, *19*, 101. doi:10.1186/s12879-019-3707-y.

Templeton, A., Guven, S. T., Hoerst, C. et al. (2020). Inequalities and identity processes in crises: Recommendations for facilitating safe response to the covid-19 pandemic. *The British journal of social psychology*, *59*, 674–685. doi:10.1111/bjso.12400.

Tryner, J., Mehaffy, J., Miller-Lionberg, D. et al. (2020). Effects of aerosol type and simulated aging on performance of low-cost pm sensors. *Journal of Aerosol Science*, *150*, 105654. doi:10.1016/j.jaerosci.2020.105654.

Zhang, R., Li, Y., Zhang, A. L. et al. (2020). Identifying airborne transmission as the dominant route for the spread of covid-19. *Proceedings of the National Academy of Sciences of the United States of America*, *117*, 14857–14863. doi:10.1073/pnas.2009637117.